NASA CR-179497

CLOSED-DRIFT THRUSTER INVESTIGATIONS

Prepared for

LEWIS RESEARCH CENTER
NATIONAL AERONAUTICS AND SPACE ADMINISTRATION
GRANT NSG 3011

June 1986

Raymond S. Robinson, Terry D. Schemmel,
and Michael J. Patterson

Department of Physics
Colorado State University
Fort Collins, Colorado

NASA CR-179497

CLOSED-DRIFT THRUSTER INVESTIGATIONS

Prepared for

LEWIS RESEARCH CENTER
NATIONAL AERONAUTICS AND SPACE ADMINISTRATION
GRANT NSG 3011

June 1986

Raymond S. Robinson, Terry D. Schemmel,
and Michael J. Patterson

Department of Physics
Colorado State University
Fort Collins, Colorado

1. Report No.	2. Government Accession No.	3. Recipient's Catalog No.
NASA CR-179497		

4. Title and Subtitle	5. Report Date
Closed-Drift Thruster Investigations	June 1986
	6. Performing Organization Code

7. Author(s)	8. Performing Organization Report No.
Raymond S. Robinson, Terry D. Schemmel, and Michael J. Patterson	
	10. Work Unit No.

9. Performing Organization Name and Address	11. Contract or Grant No.
Physics Department Colorado State University Ft. Collins, CO 80523	NSG 3011
	13. Type of Report and Period Covered
12. Sponsoring Agency Name and Address	Contractor Report
National Aeronautics and Space Administration Lewis Research Center Cleveland, OHIO	14. Sponsoring Agency Code

15. Supplementary Notes

16. Abstract

This report outlines recent data obtained from a second-generation closed-drift thruster design, employing Hall current acceleration. This type device is emphasized for electric propulsion for geocentric mission applications. Because geocentric mission profiles are best achieved with a specific impulse range of 1000-2000 s, closed-drift thrusters are well-suited for this application, permitting time-payload compromises intermediate of those possible with either electrothermal or electrostatic devices. A discussion is presented of the potential advantages of using a 1000-2000 s device for one-way orbit-raising of nonpower payloads. Because closed-drift thruster operation is not space-charge limited, and requires only one power circuit for steady-state operation, their application is technically advantageous. Beam, plasma and thrust characteristics are detailed for a range of operating conditions.

17. Key Words (Suggested by Author(s))	18. Distribution Statement
Electric Propulsion Plasma Thruster Mission Analysis	Unclassified - unlimited

19. Security Classif. (of this report)	20. Security Classif. (of this page)	21. No. of pages	22. Price*
Unclassified	Unclassified	46	

*For sale by the National Technical Information Service, Springfield, Virginia 22161

TABLE OF CONTENTS

I. INTRODUCTION

This report outlines recent work on a second-generation closed-drift thruster design, employing Hall current acceleration. Renewed research interest in this type device has been generated because of a shift in emphasis of electric propulsion to geocentric mission applications. Because geocentric mission profiles are best achieved with a specific impulse range of 1000-2000 s, closed-drift thrusters are suitable for this application, permitting time-payload compromises intermediate of those possible with either electrothermal or electrostatic devices. Although historically Hall-current accelerators have suffered from power efficiencies limited to ~50 percent, recent Soviet literature indicates propellant utilizations of up to 90 percent may be achieved, making thruster efficiencies of about 50 percent appear practical.[1,2] However, because closed-drift thruster operation is not space-charge limited, and requires only one power circuit for steady-state operation, their application to geocentric missions is advantageous.

This work was preceded by research on a smaller "proof-of-concept" closed-drift thruster[3,4] which employed permanent magnets to generate a radial magnetic field. Although thruster efficiencies were only on the order of .06, too low for propulsion applications, the single largest departure from expected performance was due to a low propellant utilization. It was concluded that poor propellant efficiencies were due, in part, to the low operating discharge power range of the device as well as the nonoptimized cathode-to-anode magnetic field profile. Further, Langmuir probe data indicated a potential drop of $\leq$ 25 percent of the discharge potential taking place between the anode and a

location just beyond the cathode. The second-generation device presented here was designed to improve thruster efficiencies with an enhanced understanding of the ion generation and acceleration processes involved.

II. ORBIT TRANSFER ANALYSIS

This section presents a discussion of the potential advantages of using a 1000-2000 s device for one-way orbit-raising of nonpower payloads.

Recent studies have indicated that ion thrusters are an excellent candidate device for orbit-raising applications.[5,6] Owing to their demonstrated superior efficiencies over a broad range of specific impulse, ion thrusters can deliver significant payload gains over other forms of electric and chemical propulsion for most mission scenarios. While there are clear advantages to the use of electrostatic thrusters for delivery of large payloads, closed-drift thrusters may provide time-payload compromises intermediate of those possible with either electrothermal or electrostatic devices. A closed-drift thrusters, operating at modest efficiencies, may in fact be capable of delivering large payloads more rapidly than other forms of electric propulsion. This situation arises for three reasons: (1) the maximum payload-fraction specific impulse associated with orbit-raising applications ($\Delta V \leqq 6000$ m/s) is in the 1000-2000 s range of closed-drift thruster operation; (2) the closed-drift thruster promises simplicity of design, requiring only one power circuit for steady-state operation which would translate into a specific mass roughly equivalent to electrothermal thrusters;[7] (3) closed-drift thrusters have potential lifetimes greatly

in excess of other electromagnetic or electrothermal concepts which suffer from inherent lifetime limiting erosion mechanisms.

For a one-way transfer mission with the power source included in the mass of the propulsion system, the deliverable payload fraction can be calculated from

$$\frac{M_{pay}}{M_{LEO}} = 1-(1+T_f)(1-e^{-x}) - \frac{(1-e^{-x})(gIsp)^2}{t\ 2\ \eta}(\alpha_{pow}+\alpha_{pro})\ x = \frac{\Delta V}{gIsp} \quad (1)$$

where T_f is the tankage fraction, t is the transfer time in seconds, η is total system efficiency, α_{pow} and α_{pro} are the power and propulsion system specific masses in kg/W_e, and ΔV is velocity increment in m/s Equation 1 assumes constant thrust.

Using Eq. 1, Fig. 1 - payload fraction vs. tranfer time for representative electric propulsion technologies was generated. An increment, $\Delta V \sim 6000$ m/s, was used which approximates the velocity increment to transfer from LEO-TO-GEO with plane change. Table 1 lists the assumptions made for the propulsion system of Fig. 1. The electrostatic thruster technology of Table 1 has been demonstrated[6], whereas the closed-drift thruster technology is based on theoretical performance predictions by Kaufman.[8] The electrothermal and chemical examples represent 30 kW hydrogen arcjet technology, and advanced hydrogen-oxygen system, respectively.

Figure 1 indicates that there are time-payload compromises which may be achieved with 1500 s closed-drift thruster technology. However, presentation like Fig. 1 have limitations: 1) they require assumptions regarding present or extrapolated electric propulsion technology; 2) they require selecting a specific mission profile; 3) they do not provide a comprehensive view of the relative merits (in

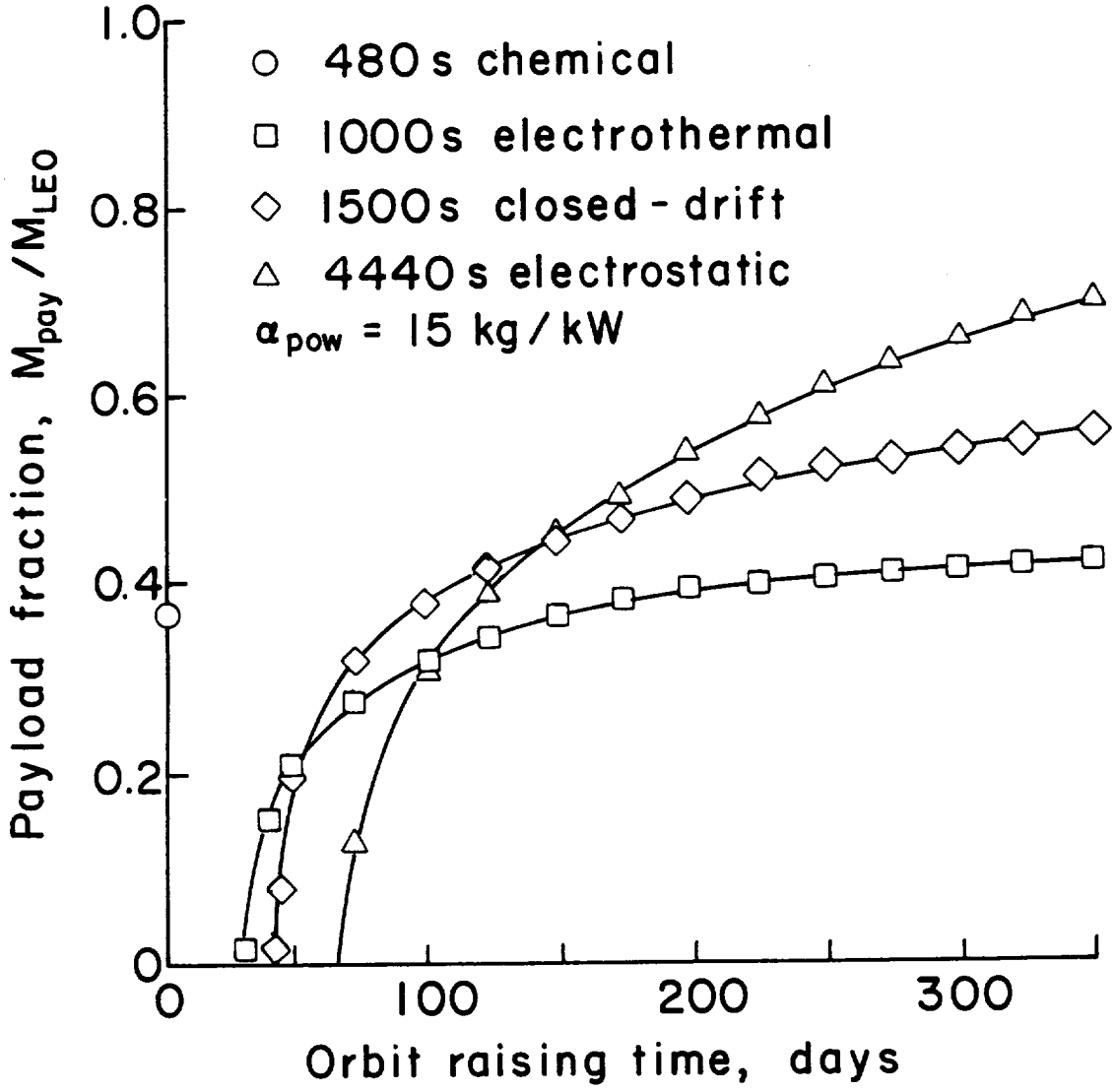

Fig. 1. Payload fraction at a function of transfer time from LEO to GEO for representative electric propulsion and chemical technologies.

Table 1. Propulsion System Assumptions

System	Isp sec	η_T	α_{pro} kg/W_e	Tankage fraction
chemical	480	--	--	0.20
electrothermal	1000	0.50	0.007	0.20
closed-drift	1500	0.45	0.007	0.09
electrostatic	4440	0.76	0.012	0.09

92% PPU efficiency assumed
α_{pow} = 15 kg/kW_e

terms of payload delivery capability) of electric and chemical propulsion systems for various orbit-raising missions.

In the spirit of Brophy and Wilbur's work on ion thruster analysis,[9] it is desirable to use the mission analysis to determine the most desirable electric propulsion system characteristics to accomplish an orbit-raising mission profile; these characteristics being the total propulsion system efficiency, and the specific impulse. For electric propulsion systems to be considered for these missions, they must be able to: 1) deliver significantly higher payloads than advanced chemical systems; 2) deliver these payloads in moderate transfer-times. With this in mind, it is interesting to calculate the system efficiency-specific impulse combinations required of an electric propulsion system to significantly increase payload delivery capability over advanced chemical systems for various orbit-raising missions. Table 2 presents orbit-raising information for transfers from LEO to 6-, 12-, 18-, and 24-hour orbits. Final orbit altitudes, impulsive-burn velocity increments (chemical system 2-burn transfer and circularization) and the equivalent-mission electric propulsion velocity increments (without plane change) are listed. These deployments are

Table 2. Orbit-Raising Missions

Mission Development from LEO (300 km) to:	Chemical Propulsion Velocity Increment, m/s	Chemical Propulsion Payload Fraction, M_{pay}/M_{LEO}	Electric Propulsion Velocity Increment, m/s	Electric Propulsion 15% Increase in Payload Fraction Chemical, M_{pay}/M_{LEO}	Electric Propulsion Corresponding Increase in Payload Mass, %
6-hr orbit 10,400 km	2710	0.47	2850	0.62	32
12-hr orbit 20,200 km	3470	0.37	3860	0.52	40
18-hr orbit 28,500 km	3750	0.34	4350	0.49	44
24-hr orbit 35,900 km	3900	0.32	4660	0.47	46

representative of the range of velocity increments for orbit-raising. Also listed are the payload fractions for each mission for an advanced chemical system (assuming 20 percent tankage and structure), the 15 percent higher deliverable payload fraction requirement of electric propulsion to be competitive to the chemical system, and the consequent increase in payload. The selection of an increase in payload fraction from chemical to electric propulsion of 15 percent was somewhat arbitrary. Although a more demanding increase in payload fraction may be required for electric propulsion systems to replace chemical, a 15 percent payload fraction increase permits modest increases in payload mass at low velocity increments (25 percent payload mass increase at ΔV =2000 m/s) and large payload mass increases at higher velocity increments (210 percent payload mass increase at ΔV = 6000 m/s).

Given the payload fraction requirements for electric propulsion in Table 2, propulsion system performance requirements can be calculated for each orbit-raising mission using Eq. 1. The results are presented

in Figs. 2 and 3. In Fig. 2, the system efficiency-specific impulse combinations for a LEO-to-6 hr orbit are presented. The curves represent lines of constant payload fraction, constant transfer-time. As an example, the 75 day transfer line and the horizontal efficiency line at unity bound the region in which possible efficiency-specific impulse combinations provide ≧ 15 percent increase in payload fraction over an advanced chemical system, with a 75 day payload deployment. Similarly, the region bounded by these two lines may be interpreted as the possible efficiency-specific impulse combinations which could deploy a 62 percent payload fraction more rapidly than 75 days, as indicated by the 50 day transfer line. For the power and propulsion system specific masses indicated, there were no solutions for a 25 day payload deployment. Similar results for a LEO-to-24 hr orbit deployment are presented in Fig. 3.

The characteristic curves of Figs. 2 and 3 reflect the propellant mass penalty at low specific impulse, and the propulsion system mass penalty at high specific impulse. The figures indicate that propulsion system operation in the 1000-2000 s specific impulse range requires significantly less system efficiency to accomplish an orbit-raising mission than that required of operation below 1000 s or above 2000 s for the same mission. The propulsion system specific mass and tankage fraction used are representative of closed-drift thruster technology. Curves of this type were also generated for representative electrothermal and electrostatic thruster technologies, data for which are presented in Table 3. The electrothermal and electrostatic thruster technologies require higher system efficiencies than those of the closed-drift thruster technology for each orbit-raising mission. These

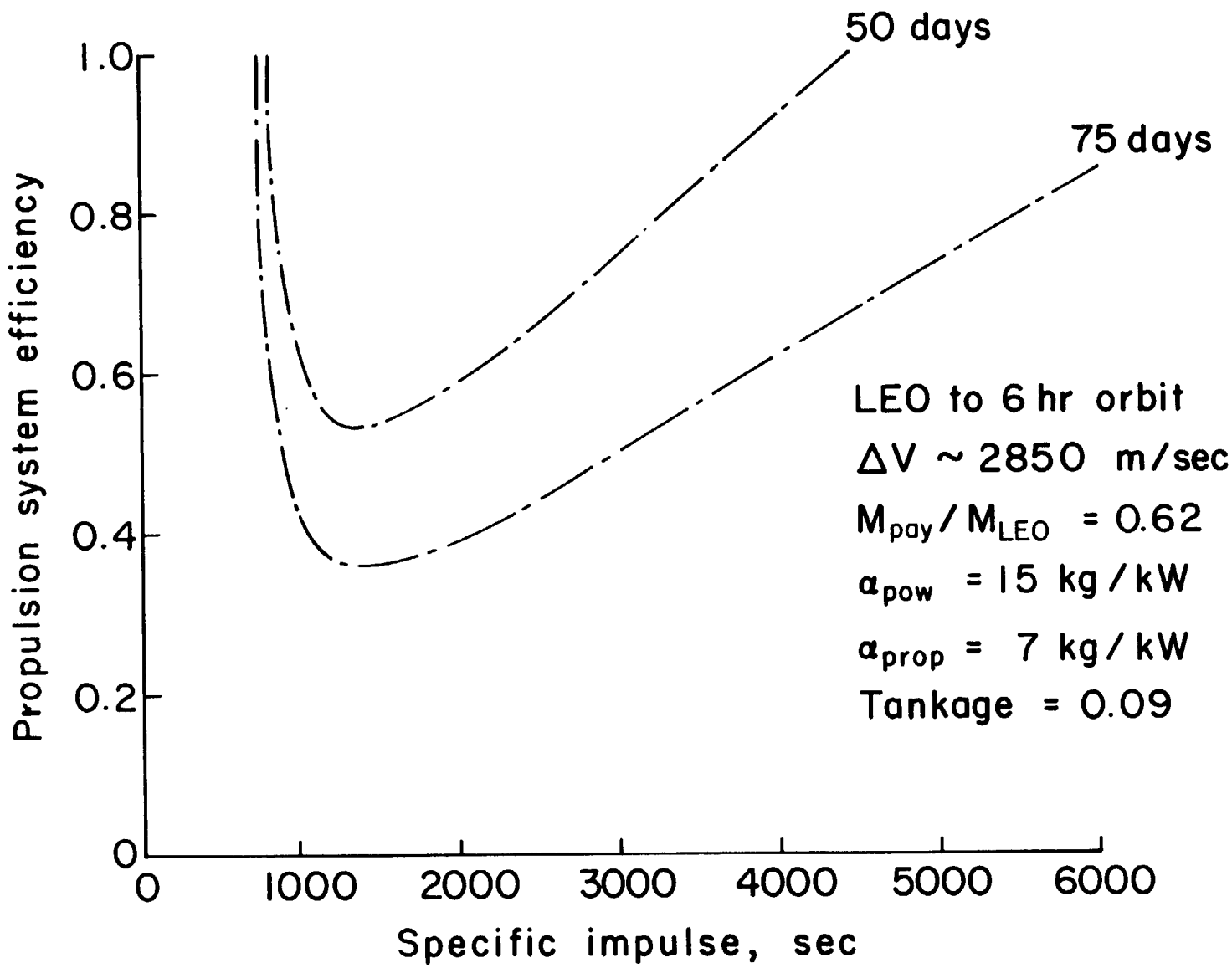

Fig. 2. Capabilities of electric propulsion for LEO to 6 hr orbit transfer.

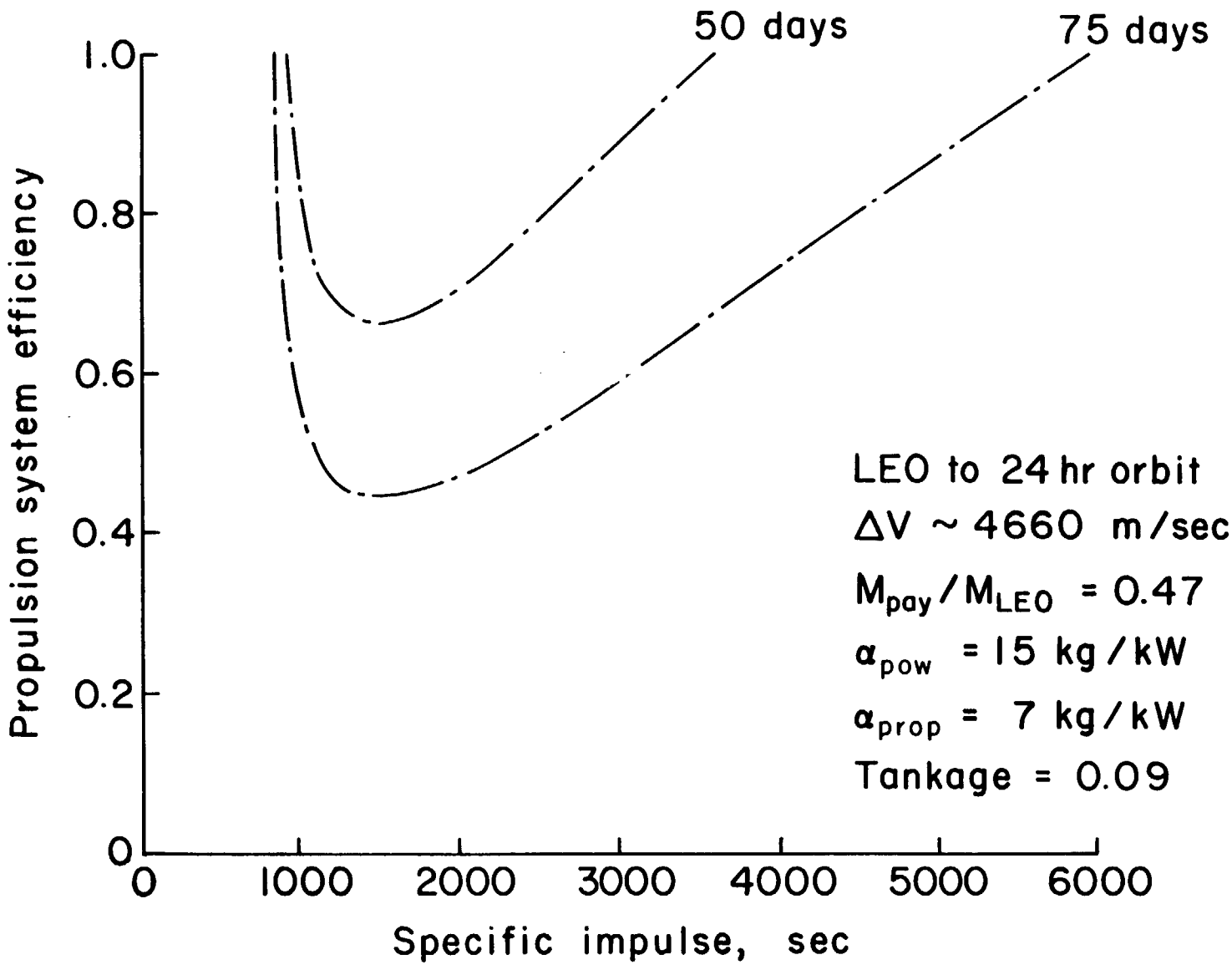

Fig. 3. Capabilities of electric propulsion LEO to 24 hr orbit transfer.

Table 3. Capabilities of Electric Propulsion for Orbit-Raising Missions

Mission Deployment from LEO (300 km) to:	Payload Fraction, M_{pay}/M_{LEO}	Specific Impulse, s	System Efficiency Requirements for Payload Deployment in 75 Days		
			Closed-Drift Thruster Technology	Electrothermal Thruster Technology	Electrostatic Thruster Technology
6-hr orbit	0.62	1000	0.42	0.57	--
		1500	0.36	0.40	0.49
		2000	0.39	--	0.53
24-hr orbit	0.47	1000	0.55	0.86	--
		1500	0.44	0.50	0.60
		2000	0.47	--	0.64

penalties are due to the requirements of cryogenic propellant storage for hydrogen-arcjet thrusters, and the relatively high propulsion system specific mass of ion thruster systems below 2000 s specific impulse.

III. APPARATUS AND PROCEDURE

Closed-Drift Thruster

A cross section of the second-generation closed-drift thruster tested is presented in Fig. 4. The closed-drift thruster employs axially symmetric electrodes and pole pieces, with the magnetic field in the radial direction and the electric field in the axial direction. The downstream magnetic pole pieces are located at y = 0 position. In terms of the coordinate y, the position of the anode can be adjusted from the -27 mm location to the -33 mm location. The acceleration channel is bounded by grounded walls that extend from -15 mm to a point just beyond the anode. The inner grounded wall has a diameter of 50 mm and the outer grounded wall has a diameter of 88.5 mm. The anode is an annular ring of width 8 mm centered between the channel walls. Operation of the closed-drift thruster was conducted with a 0.020" dia. tungsten refractory filament cathode with annular shape located at the +6 mm position. The filament cathode provides electrons for both propellant ionization and beam neutralization.

The closed-drift thruster also employs an electromagnet to vary the magnetic field profile. This provides the capability to optimize propellant efficiency at a desired operating point by more efficient use of the electron energy to produce ions. The magnetic field was analyzed for both uniformity and linearity along with nickel filing mapping of the field lines. Inspection of the field maps indicated

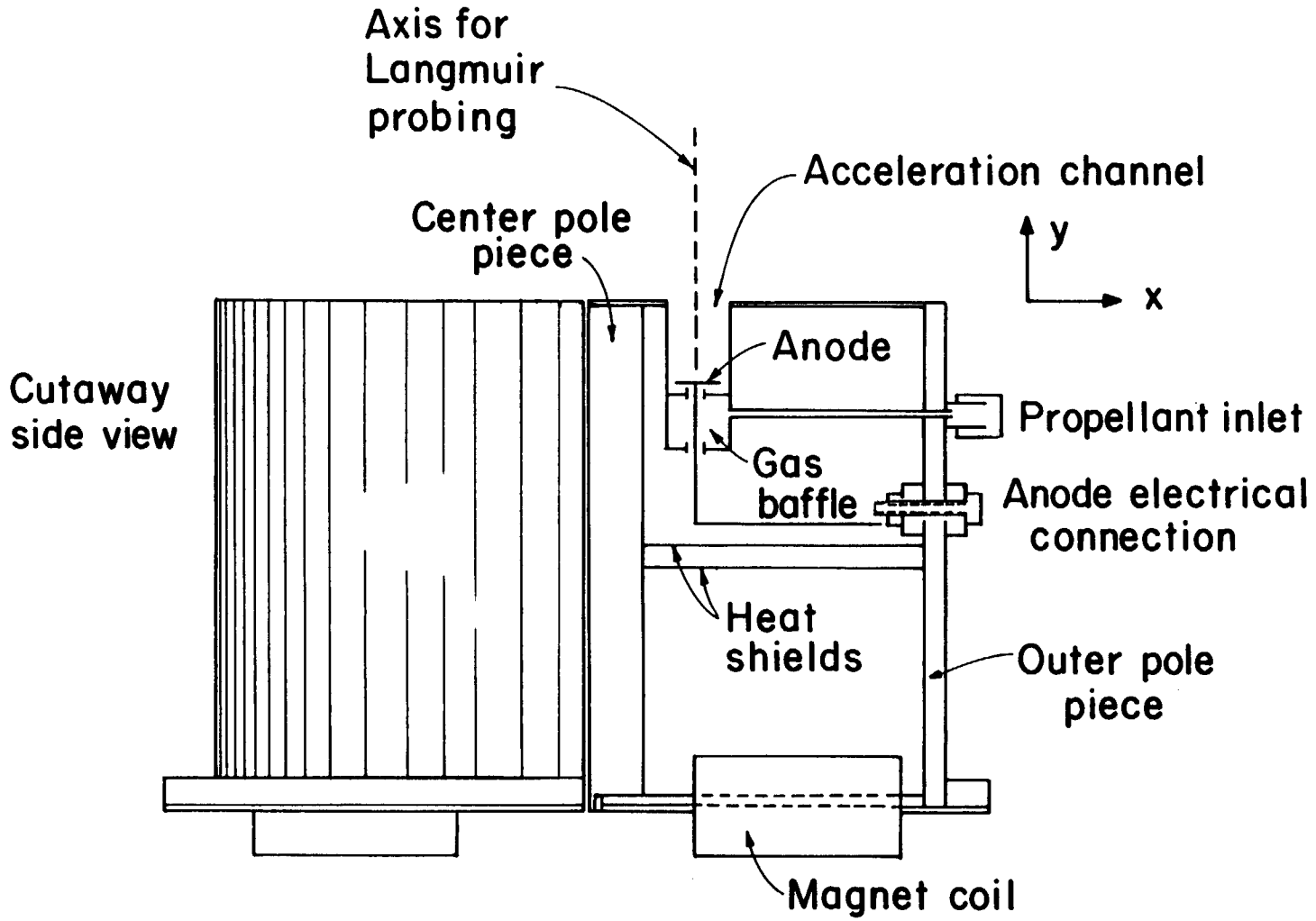

Fig. 4. Cross section of second-generation closed-drift thruster.

that the field was symmetric for opposite sides of the channel as expected. The radial magnetic field component as a function of axial position along the channel is shown in Fig. 5. The downstream pole pieces provide a factor of two in magnetic field concentration above the value found at the anode location; the field then falls rapidly toward zero in the downstream direction. This type of magnetic field variation tends to accommodate the conflicting requirements of ion production and acceleration; by permitting ion production in the low magnetic field strength region thereby reducing neutral losses, and at the same time providing a high field strength in the acceleration region which reduces electron diffusion in the upstream direction. The field was measured to be uniform azimuthally. The total magnetic field can be calculated at each point if the radial component is known and the angle that the field vector makes with the horizontal is also known. The magnetic field direction was found by taking tangents to the field lines as a number of axial locations in the channel; these data are shown in Fig. 6.

The magnetic field data of Figs. 5 and 6 can be scaled linearly with magnet current to any other field condition. To demonstrate that none of the magnetic circuit components saturated to cause a nonlinear condition, the field was measured at the two points of greatest concentration for the inner and outer pole piece assemblies. The field was linear with magnetic current over the entire range of field strengths utilized in this study.

The second-generation thruster was also designed with greater heat rejection capability than its predecessor. This was motivated by the fact that high discharge power levels are required to attain the A/cm^2

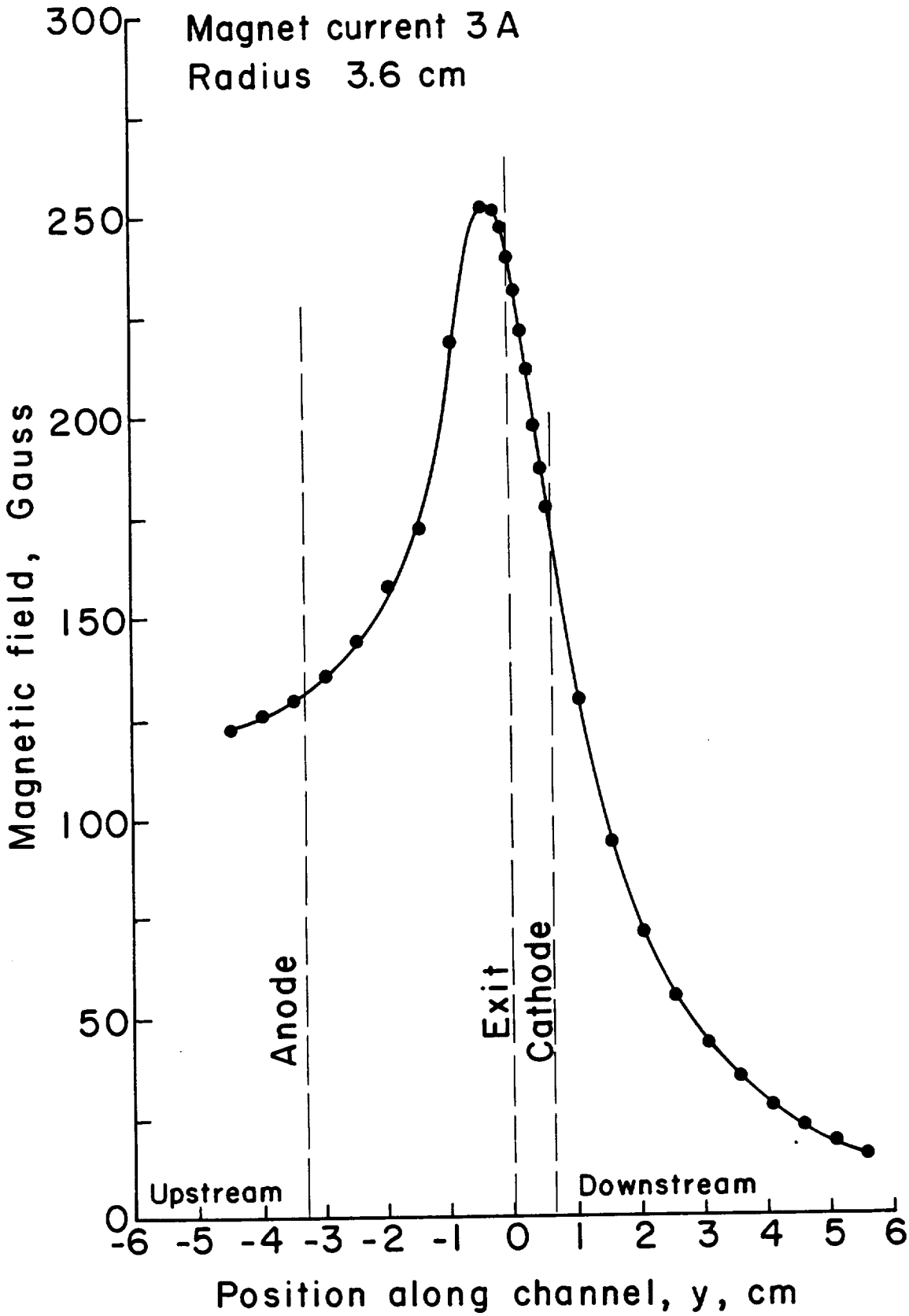

Fig. 5. Radial magnetic field component as a function of position along channel.

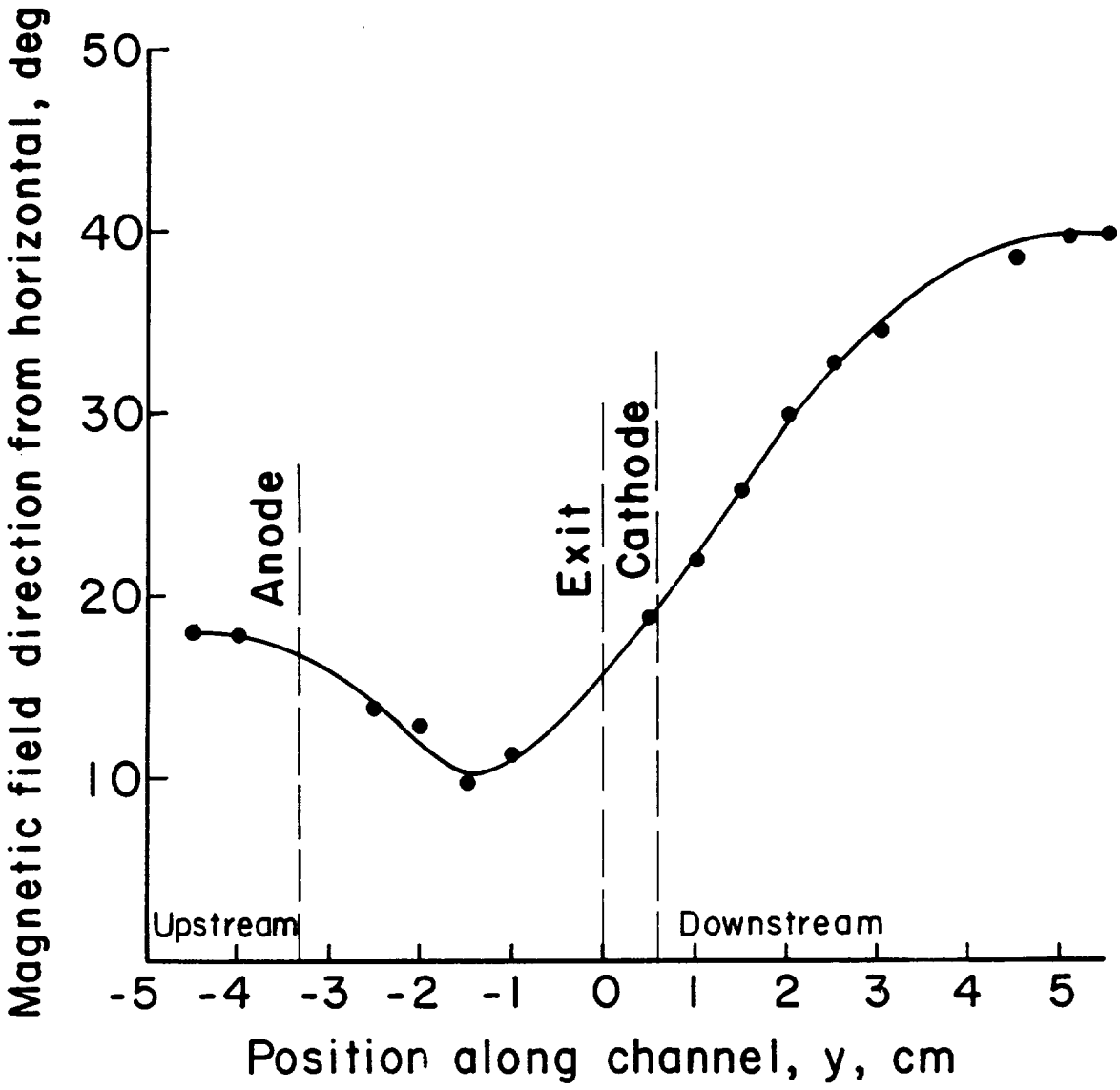

Fig. 6. Magnetic field direction as a function of channel position.

range for the extracted ion beam, if acceptable propellant utilization is to be obtained. A thorough treatment of the theory of electron diffusion, ion production, and acceleration processes in closed-drift thrusters which motivated some design considerations of this device, can be found in work by Kaufman.[8,10]

Plasma Diagnostics

A Faraday probe system was built to provide ion current density and energy distribution information about the beam from the thruster. The Faraday probe, constructed of a pyrolytic graphite screen and current collecting element, was mounted on a motorized x-axis (Fig. 4) drive which could sweep across the downstream plane of the thruster. The collected current was measured as a voltage drop across a precision sensing resistor in series with the collecting element. This voltage was then displayed using an x-y recorder along with a signal proportional to either probe position for a beam current density profile or proportional to probe bias for an energy analysis.

The total beam current was determined by integrating the beam current density profiles. Corrections to the beam current values for charge-exchange was negligible due to the position of the Faraday probe (18.6 cm downstream of the thruster) and the low operating facility pressures.

The ion beam energy distribution was determined from the current measured to the Faraday probe as a function of retarding bias on the probe. The derivative of this characteristic was calculated as a function of energy; these derivatives were then fit to a function consisting of a constant baseline current density plus a Gaussian profile centered about the peak energy. There were four free

parameters in the curve fit: the value of the baseline current density, the mean value of the Gaussian, the amplitude of the Gaussian, and the width of the Gaussian. The parameters of the curve fit were chosen to minimize the sum of the magnitudes of the deviations of data points from the fit line. This was done in preference to a least squares fit because least squares is inappropriate for data whose variation does not follow a simple normal distribution. An iterative procedure was followed until all four parameters were determined within fixed tolerances.

Detailed plasma potential and plasma density information along the ion acceleration region of the thruster channel was provided by a Langmuir probe system. Using a motorized y-axis drive, a spherical Langmuir probe was positioned along the channel (see Fig. 4) at 4 mm increments from the anode to a point 40 mm beyond the cathode. Further downstream, data were taken at 1 cm increments to a distance of approximately 13 cm. Plasma properties were determined from Langmuir probe characteristics using a proportional variation fit of the retarding-field region. The plasma potential and electron saturation current were then determined from the simultaneous solution of the retarding-field region fit, and a fit of the acceleration region.

With both Faraday and Langmuir probe diagnostics, ion production along the channel as judged from the beam energy analysis could then be correlated with plasma density and electron energy.

Test Facility

Closed-drift thruster research was conducted at the Colorado State University Plasma Physics Laboratory. The thruster was tested in a 2.4 m x 4.0 m vacuum facility with sufficient pumping capability to

maintain pressure in the low 10^{-5} Torr range during operation. Two 100 V/100 A laboratory power supplies were used for thruster operation; one discharge supply, and one filament cathode supply.

IV. RESULTS AND DISCUSSION

Discharge and Beam Characteristics

For ease of operation, the closed-drift thruster studies presented here were conducted with a refractory filament cathode. However more recent studies at NASA-Lewis Research Center have demonstrated closed-drift thruster operation with a hollow cathode. Starting the discharge required filament cathode heater currents of 65-85 A at anode voltages of 80-100 V. Preliminary thruster operating characteristics were measured in terms of discharge voltage as a function of Argon propellant flow. This was done for a range of discharge currents from 2 A to 10 A at 1 A intervals for several magnet currents. Figure 7a shows the variation of discharge voltage with Argon flow for the 2, 4, 6, and 8 A current levels for a magnet current of 0.2 A. The data presented in the figure are for two thruster configurations, a short channel configuration of channel length 27 mm, and a long channel configuration of 33 mm. The general feature of all the data is the normal increase in channel conductivity with increasing propellant flow. The operating regime was limited in one way by the maximum voltage of the discharge power supply. Another limitation was the minimum flow required to sustain a discharge. In all cases, a flow greater than 20 sccm was required for operation. Attempts to reduce indicated flow below 25 sccm were made at all conditions not limited by discharge voltage. The discharge typically was extinguished at about 23-24 sccm. The data also indicates an increase in channel conductivity going from the short

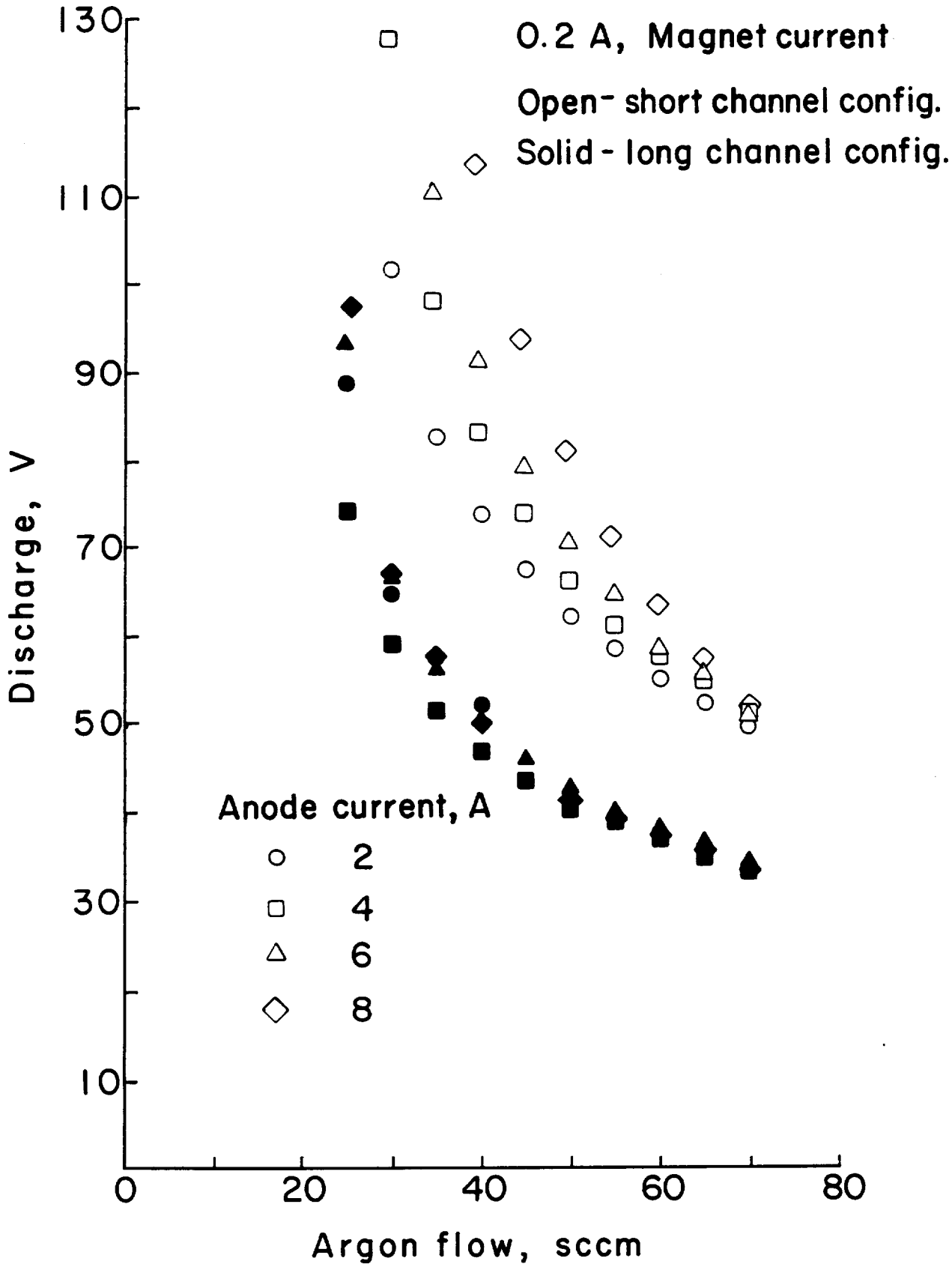

Fig. 7a. Voltage as a function of flow for representative anode currents.

channel to the long channel configuration. This increased channel conductivity was interpreted as an increase in ionization efficiency associated with a larger ion production volume for the long channel configuration. This was supported by the observation of a more well-collimated ion beam for long channel operation.

Figure 7b shows the variation of the mean energy of the beam ions (see Table 5) as a function of magnet current. As the impedance of the channel is increased, the voltage drop across the field region increases resulting in a greater mean energy for the ions in the beam. Figure 7c shows the variation of the mean energy of the beam ions as a function of argon flow. Greater flows allowed more ionization and more conductivity; the greater conductivity in the channel reduced the voltage drop thus reducing the average ion energy. Another factor contributing to the reduction in ion energy is the relatively larger fraction of ions produced downstream of the magnetic field region.

Figure 8 presents the long channel variation of discharge voltage with Argon flow for 0.2, 0.6, and 1.0 A magnet current levels for a 6 A discharge. The 0.2, 0.6, and 1.0 A magnet currents were associated with a magnetic field strength of approximately 15, 20, and 40 G, respectively, for a downstream field maximum location near the inner pole piece. As indicated in Fig. 8, the spread in discharge voltages for increasing current at a constant flow increases with higher magnet currents reflecting the greater electron impedance in the channel at higher magnetic fields. The spread in discharge voltage was smallest for the long channel configuration at the lowest magnetic field.

Preliminary analysis of beam characteristics were conducted for a range of discharge and magnet currents. Figure 9 presents beam current

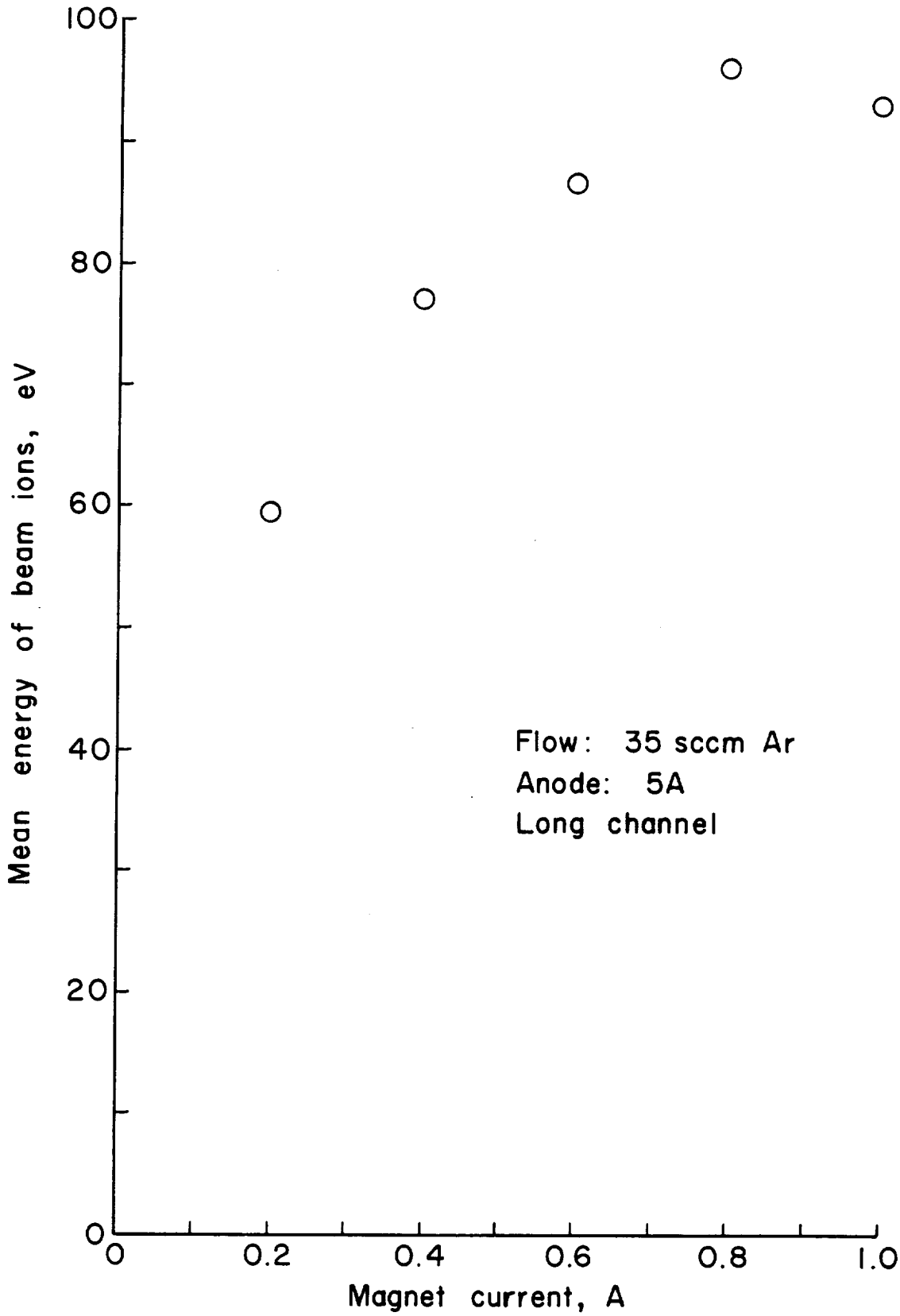

Fig. 7b. Mean energy of beam ions as a function of magnet current.

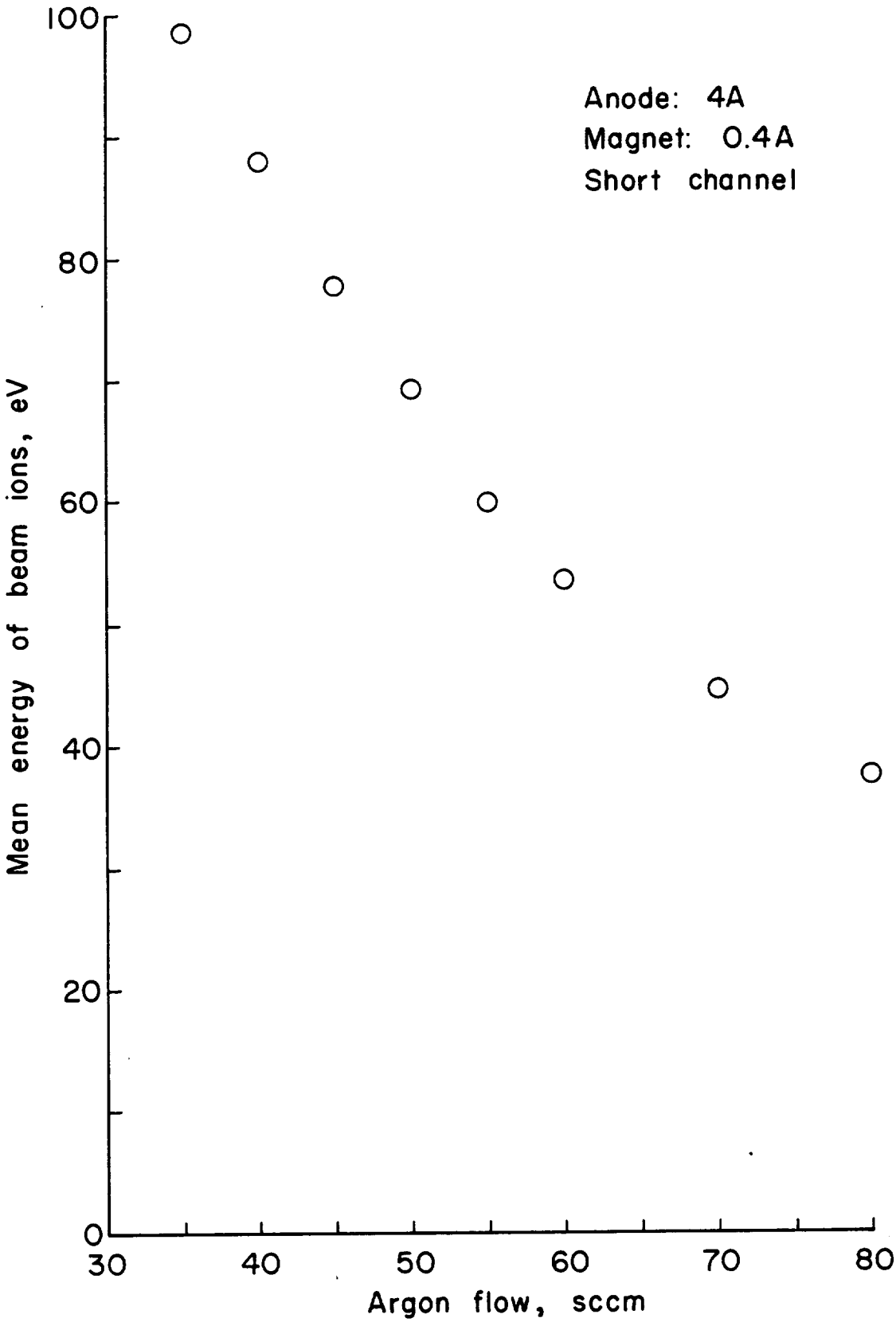

Fig. 7c. Mean energy of beam ions as a function of argon flow.

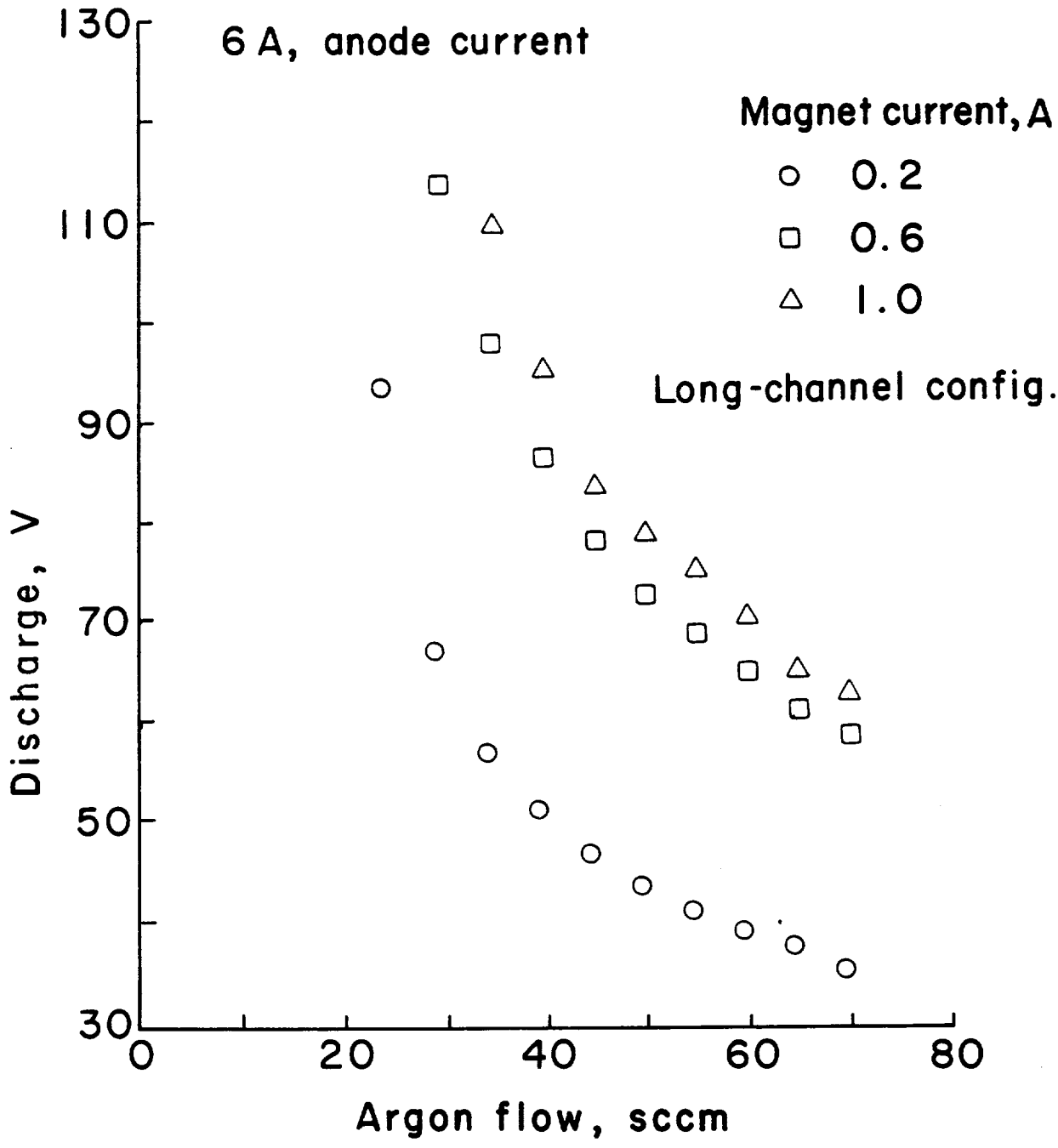

Fig. 8. Voltage as a function of flow at different magnet currents.

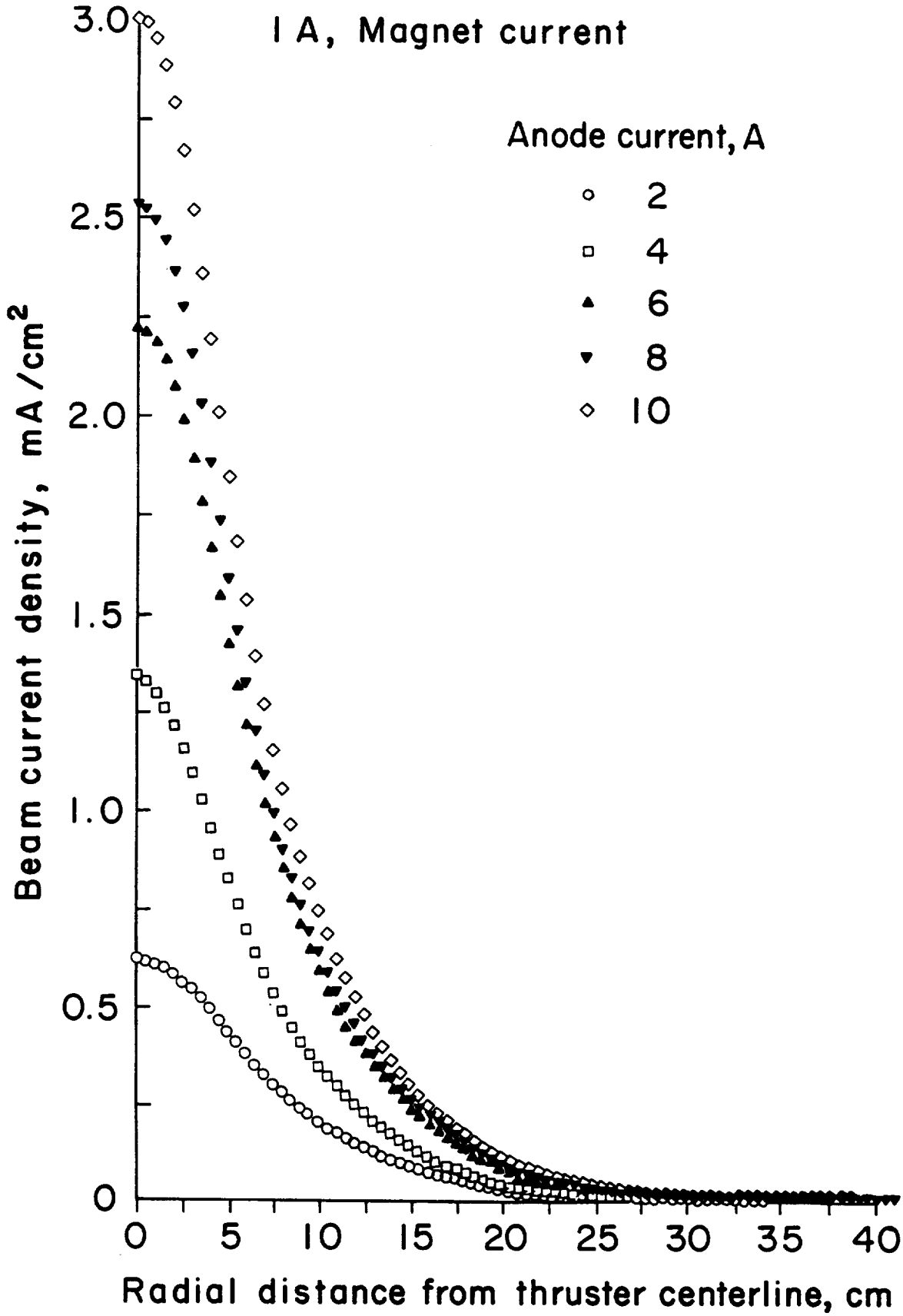

Fig. 9. Beam current density profiles for representative anode currents

density profiles for 2, 4, 6, 8 and 10 A discharge currents at 1.0 A magnetic current for the short channel configuration with 60 sccm Argon flow. Since no asymmetries in beam profiles with respect to the centerline of the thruster were observed, the Faraday probe system was positioned as to allow 40 cm of probe travel on one side of the thruster centerline. As seen in Fig. 9, the shape of the profile changes with increasing discharge current. The increase in current density is greater near the center of the beam than it is at larger radii when compared to current densities at lower discharge currents. The ion generation process in the channel appears to become more effective at higher power levels relative to generation further downstream. Integrated beam current data and thruster operating conditions for the beam current density profile of Fig. 9 are presented in Table 4. An analysis of the ion beam energy distribution for the beam current density profile of Fig. 9 using the technique outlined in the previous section is presented in Table 5. E_{mean} is the mean energy of the Gaussian, σ is the standard deviation of the Gaussian, and E_m/σ and E_m/V_{dis} are the ratios of the mean energy of the Gaussian to the standard deviation and the discharge voltage respectively. The

Table 4. Argon Integrated Beam Current Data

Discharge Current A	Cathode Emission Current, A	Discharge Voltage, V	Integrated Beam Current, mA	$\frac{J_{beam}}{J_{dis}}$
2.0	2.5	88	213	0.107
4.0	5.0	90	366	0.092
6.0	7.5	103	620	0.103
8.0	10.0	120	688	0.086
10.0	12.5	125	804	0.080

Table 5. Ion Beam Energy Distribution

Discharge Current, A	E_{mean}, eV	σ, eV	E_{mean}/σ	E_{mean}/V_{dis}
2.0	61.8	13.2	4.68	0.70
4.0	64.2	14.9	4.31	0.71
6.0	78.9	16.9	4.65	0.77
8.0	94.3	17.0	5.54	0.79
10.0	101.5	14.8	6.87	0.81

behavior of the beam energy distribution with increasing power exhibits a fairly regular progression or uniform behavior in all parameters. The mean energy of the beam represents an increasing fraction of the discharge voltage for higher discharge voltages probably partly a result of a decreased charge exchange cross section at higher energies. A number of processes probably contribute to the generation of a Gaussian profile for the beam energy distribution. The plasma potential at which ions are created will determine their maximum total energy but collisional processes and charge exchange can alter the makeup of the energy distribution after the ions begin to accelerate along the channel.

Based on the initial analysis of the discharge and beam characteristics, four operating conditions of the long channel thruster were selected for Langmuir probe diagnostics of the acceleration channel, and further beam energy analysis. These thruster conditions are listed in Table 6. An Argon flow of 60 sccm was selected because it provided stable operation over a very wide range of discharge currents and voltages, as well as providing easy starts. Two magnet currents at low and high level discharge currents were selected which

Table 6. Selected Operating Conditions of Long Channel Configuration

Condition No.	Discharge Current, A	Cathode Emission A	Discharge Voltage V	Magnet Current, A
1	10	12.5	92.9±2.3	2.8
2	10	12.5	77.2±4.0	0.8
3	5	6.25	66.7±2.5	0.8
4	5	6.25	80.5±3.5	2.8

essentially bracketed the region of stable operation of the device. The low magnet current of 0.8 A provided a downstream field strength in the acceleration channel of less than 100 G, while the high current of 2.8 A provided a field strength in excess of 150 G. These four conditions were selected to aid in determining general behavior of the discharge plasma and beam with magnetic field strength and discharge current.

Plasma Properties

Detailed Langmuir probing of the thruster channel was conducted for the four selected operating conditions using the technique outlined in the previous section. The density of Maxwellian electrons in the plasma as a function of channel position is presented in Figs. 10 and 11. In Fig. 10, the equivalent magnetic field test conditions 1 and 4 are compared. The higher discharge current level of condition 1 resulted in a higher peak Maxwellian density in the acceleration channel. The contrast in electron densities for high and low discharge currents is more readily apparent in Fig. 11 which compares the lower magnetic field test conditions 2 and 3. Each of the density profiles exhibits a peaked profile in the high magnetic field acceleration

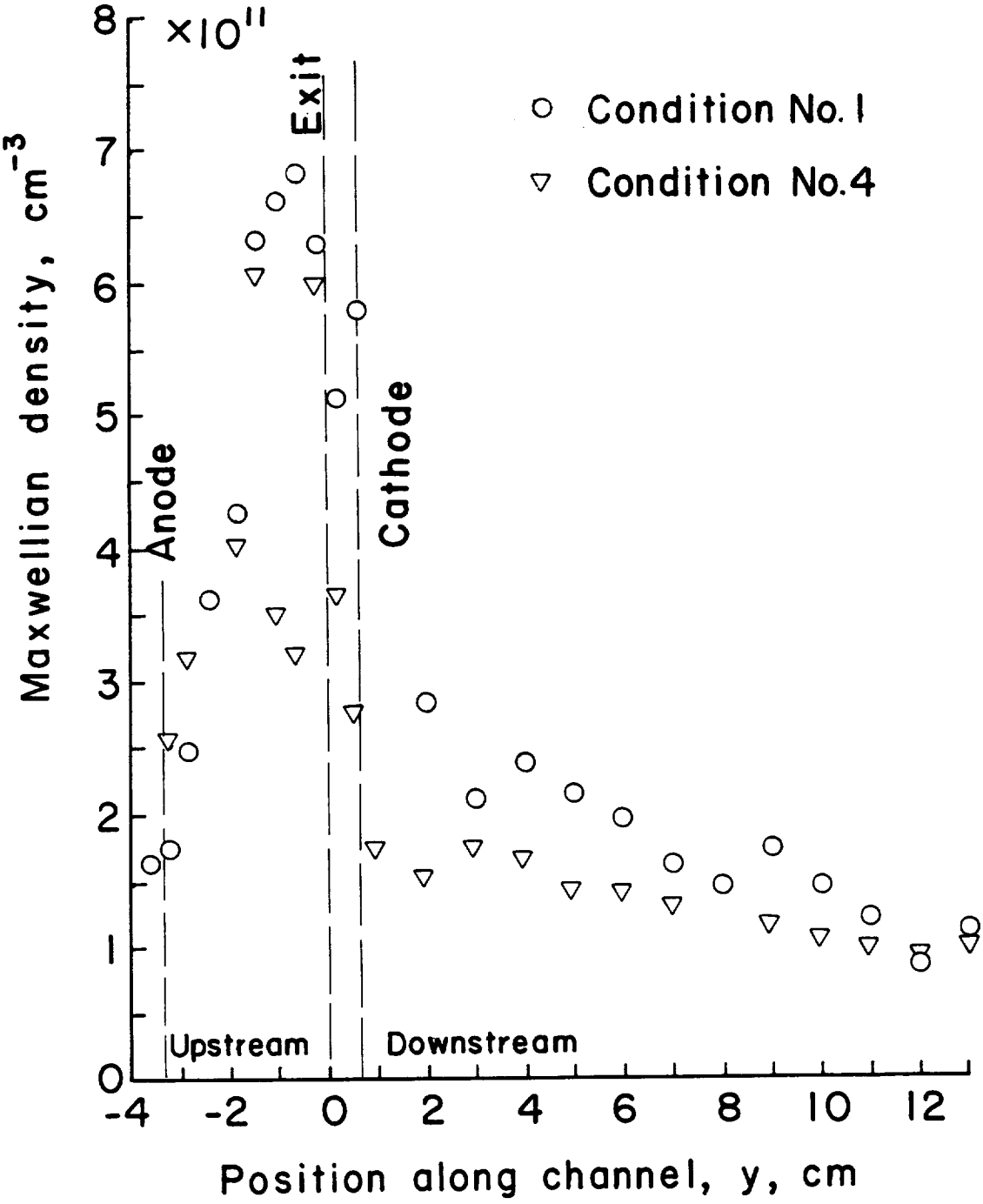

Fig. 10. Maxwellian electron density as a function of channel position, conditions 1 and 4.

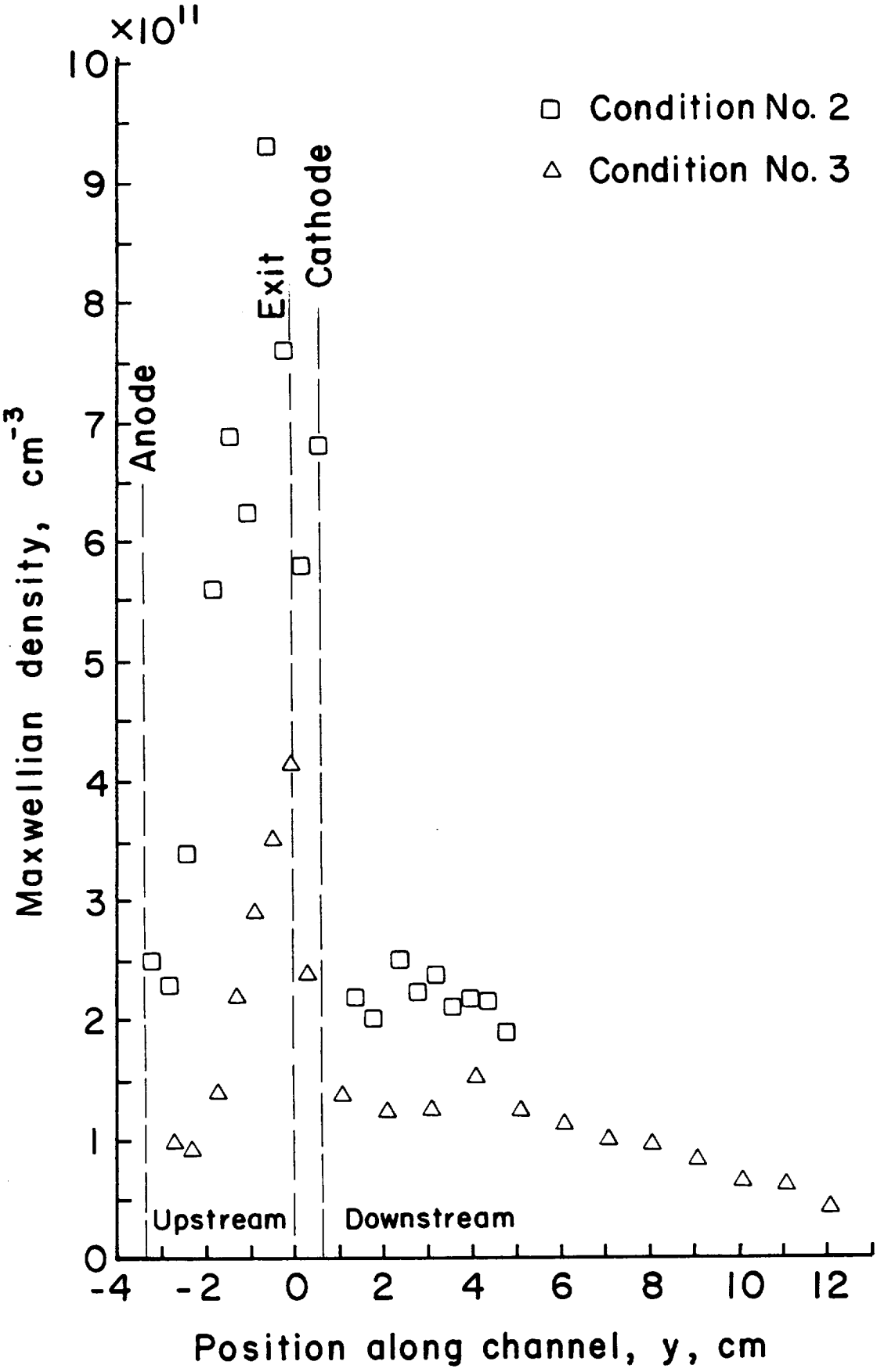

Fig. 11. Maxwellian electron density as a function of channel position, conditions 2 and 3.

region of the channel throat which drops off rapidly beyond the field region. Assuming a two group electron distribution, the primary electron densities also exhibited a peaked profile in the same region. The primary densities dropped off to approximately 10 percent of their peak density half-way up the channel, with the primary to Maxwellian electron density ratio being on the order of 11 percent for all test conditions. This indicated that the maximum ion production was taking place just inside the magnetic field with the bulk of ion production occurring downstream of the grounded channel.

Electron temperature profiles are presented in Fig. 12 for test conditions 1 and 4. Downstream, in the beam region, the electrons are fairly cool at about 2-3 eV. In the acceleration channel and ion production region the electron temperature averages about 8 eV indicating a separate population that shares in the energy gained by electrons traveling upstream. This thruster thus operates at a condition between the two theoretical extremes of 1) constant electron temperature, and 2) strict energy conservation delivering all directed electron energy as thermal energy upstream. Primary electron energies along the thruster channel were above 35 eV for all the test conditions. This energy is clearly sufficient to permit significant ionization by primaries.

The plasma potential as a function of channel position is shown in Fig. 13 for test condition 4. The potential in the beam region is about constant at 20 V for some distance from the thruster. A positive potential of a few times the electron temperature is expected in the beam region to allow for neutralization. However, facility interactions and a significant background gas density probably also contribute to

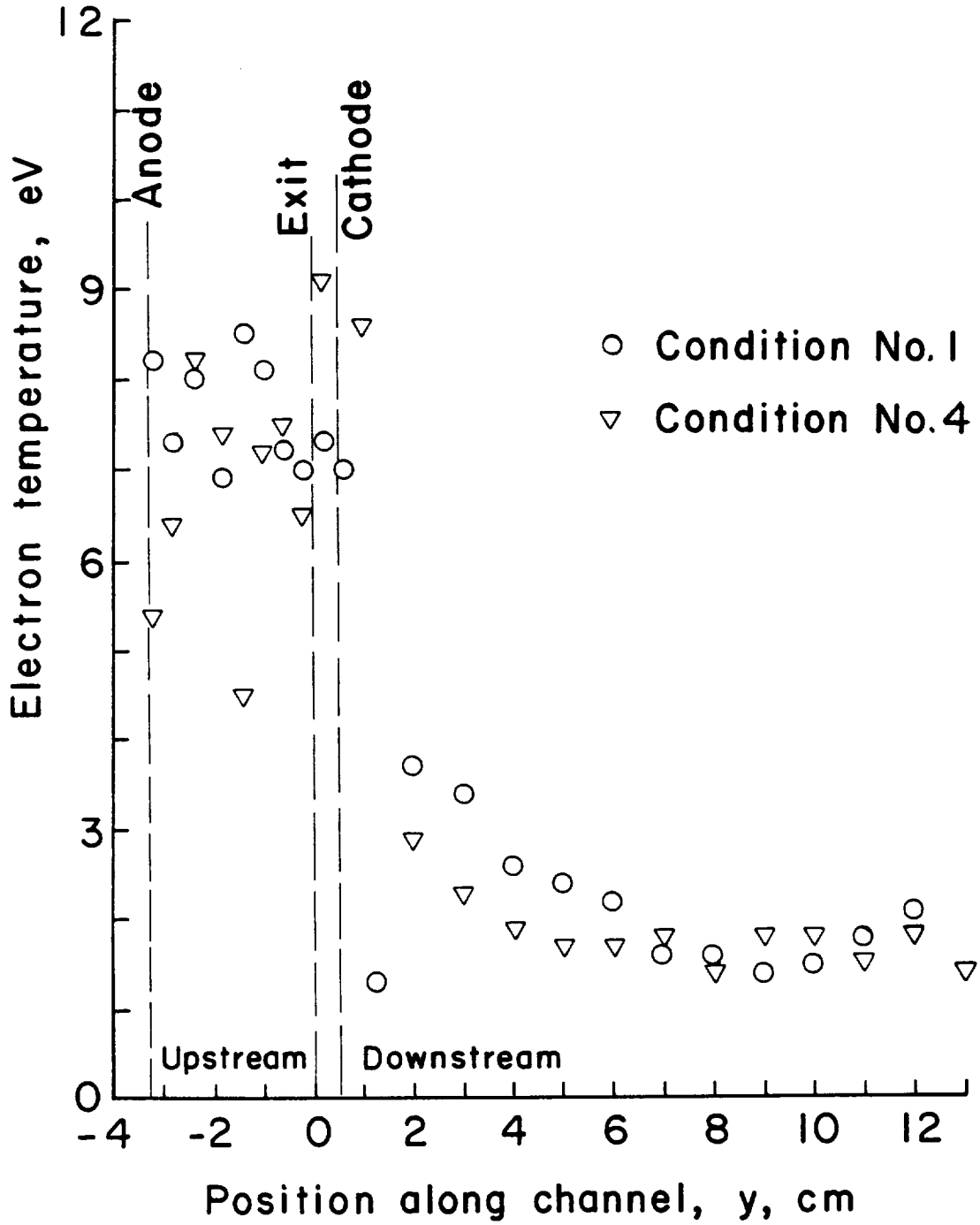

Fig. 12. Electron temperature as a function of channel position, conditions 1 and 4.

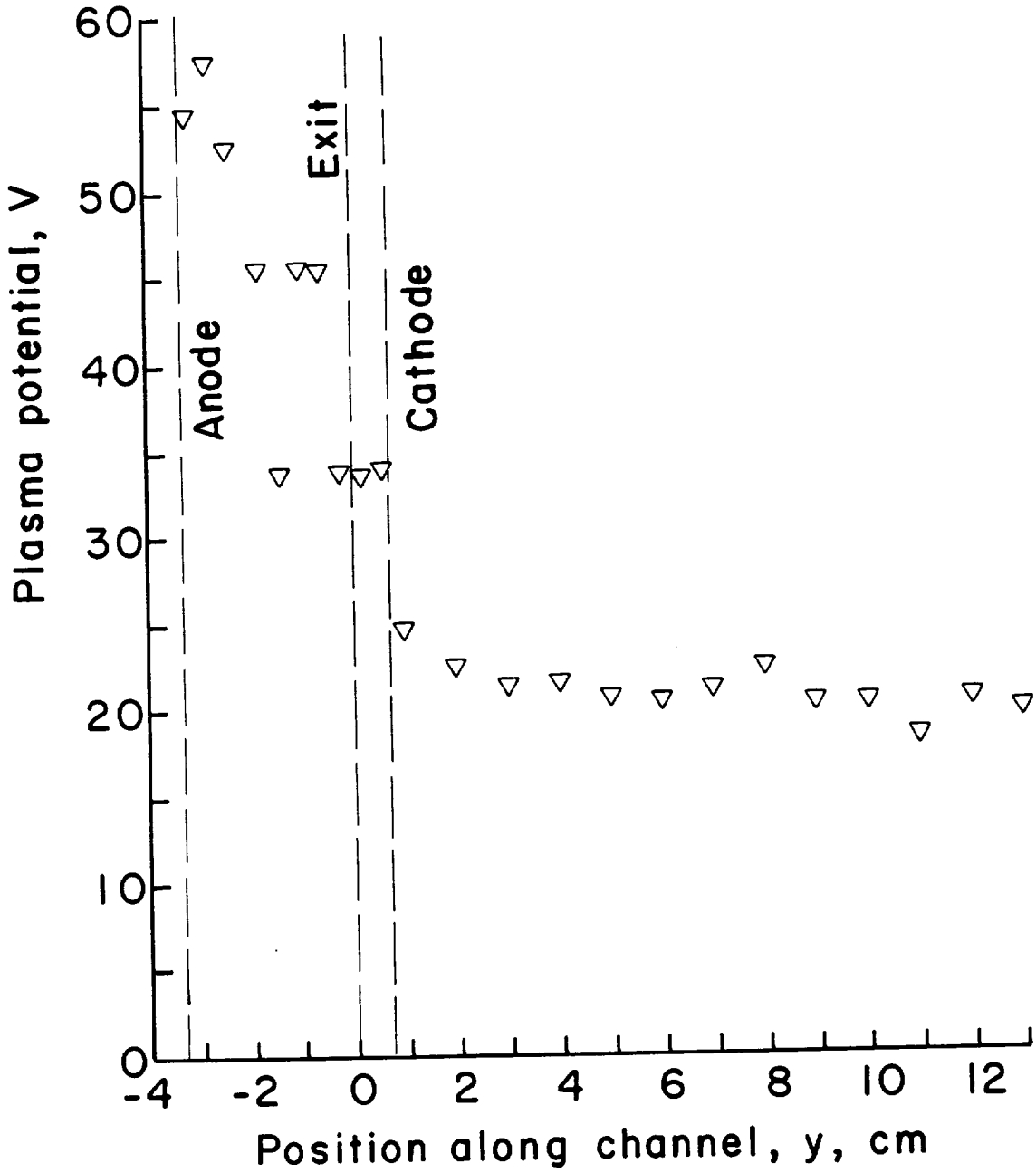

Fig. 13. Plasma potential as a function of channel position for condition 4.

raising the potential. Plasma potential rises sharply in the strongest magnetic field region where the greatest resistance to electron conduction is encountered and continues generally to rise as the anode is approached. The potential gradient increases sharply near the anode exhibiting a characteristic behavior of anode layer accelerators.

Insulated Channel Tests

Further inspection of electron temperature profiles of test conditions 2, 3, and 4 indicated a significant drop in electron temperatures at a location in the channel near the -15 mm location of the metal grounded channel walls. This indicated that the channel walls were acting as a virtual anode, thus creating a loss mechanism for the plasma. This loss mechanism in turn would account for the near-constant electron temperature observed in most of the channel. Because of this, dielectric cylinders of pyrex were placed in the thruster to line the inner and outer metal channel walls. This was in hopes of conserving electron energy which would result in a temperature gradient and a near discontinuous plasma potential jump at the positive end of the acceleration channel. This operation would then correspond to a closed-drift anode-layer accelerator which has inherent efficiency advantages over that of the closed-drift Hall-current accelerator.

Figure 14 presents Maxwellian electron density measurement for condition 4 for the insulated channel configuration. These are plotted against information from the earlier grounded channel tests at the same condition. As indicated, the pyrex channel data is much less peaked in the acceleration region. The ratio of primary to Maxwellian electron densities along the channel were much higher for the pyrex channel. The ratio peaked in the acceleration channel at 50 percent and dropped

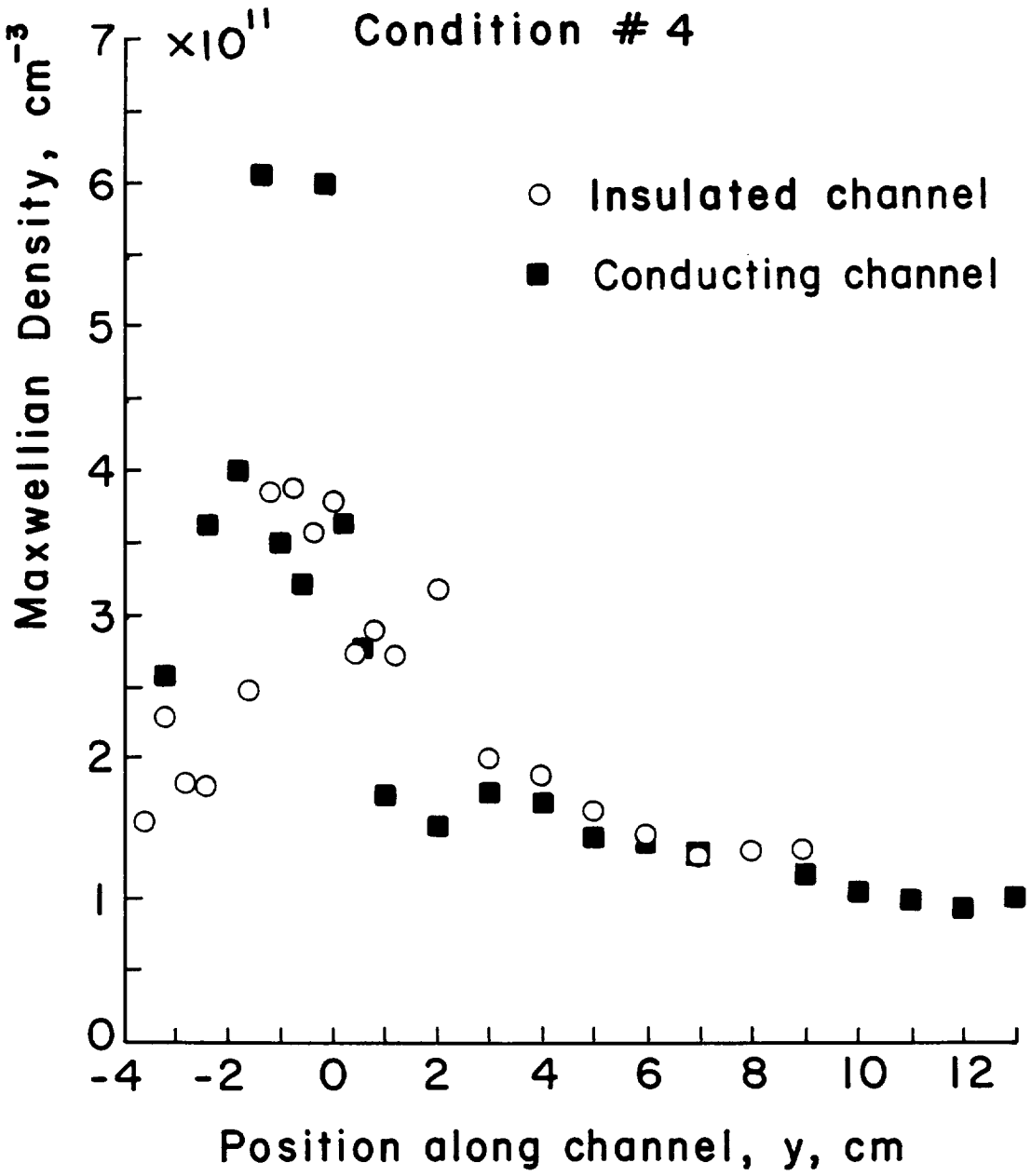

Fig. 14. Maxwellian electron density comparison for insulating and conducting channels.

off toward the anode to about 10 percent, whereas the grounded walls had a near constant ratio across the channel of about 11 percent. This increased ratio was a consequence of much higher primary electron densities measured in the acceleration region for the pyrex wall tests.

Electron temperature profiles are presented in Fig. 15 for pyrex and grounded channel condition 4 tests. The temperature profile for the pyrex walls indicates a steep gradient from the acceleration region to the anode. This is in contrast to the profile found in the grounded channel tests. This indicates that the insulated channel thruster operates at a condition much closer to the theoretical extreme of strict energy conservation. The primary electron energies measured along the insulated channel were approximately 10 eV above those measured for the metal channel.

The plasma potential as a function of channel position for condition 4 for the insulated and metal channel configurations is presented in Fig. 16. As indicated, a much steeper gradient in potential was observed in the insulated channel configuration. A near discontinuous jump in potential at the positive end of the acceleration channel also occurred. Figure 17 shows that the ratio of plasma potential to discharge voltage linearly increases across the channel to the anode, with the insulated channel having a steeper slope than the grounded channel test. Figure 18 presents normalized plasma potentials as a function of channel position for the four test conditions with grounded channel, and condition 4 with the insulated pyrex channel. The profiles were normalized so that the external behavior downstream of the thruster was the same. Two interesting points are illustrated by Fig. 18. The first is that the magnitude of the plasma potential is

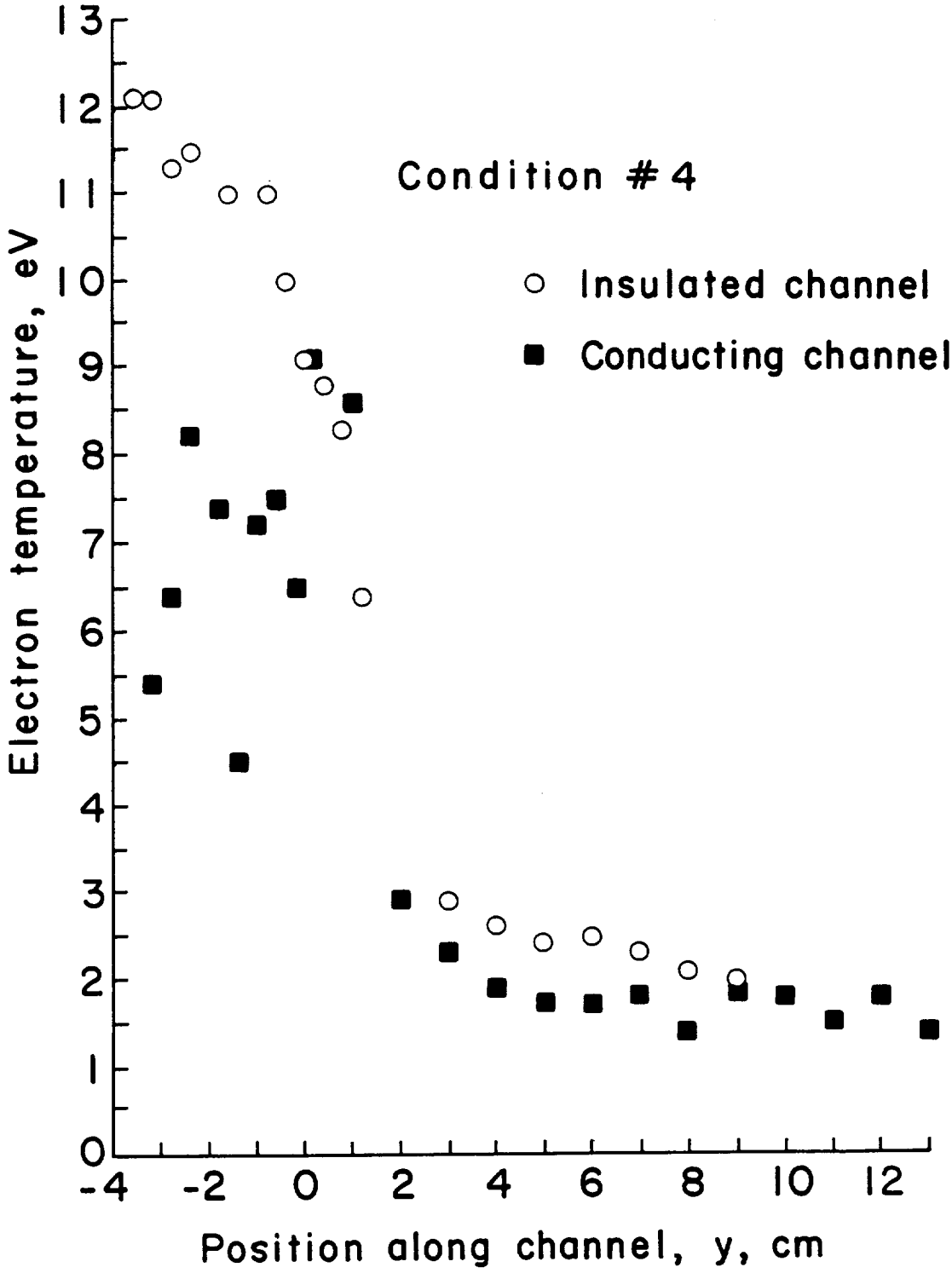

Fig. 15. Electron temperature comparison of insulated and conducting channel operation.

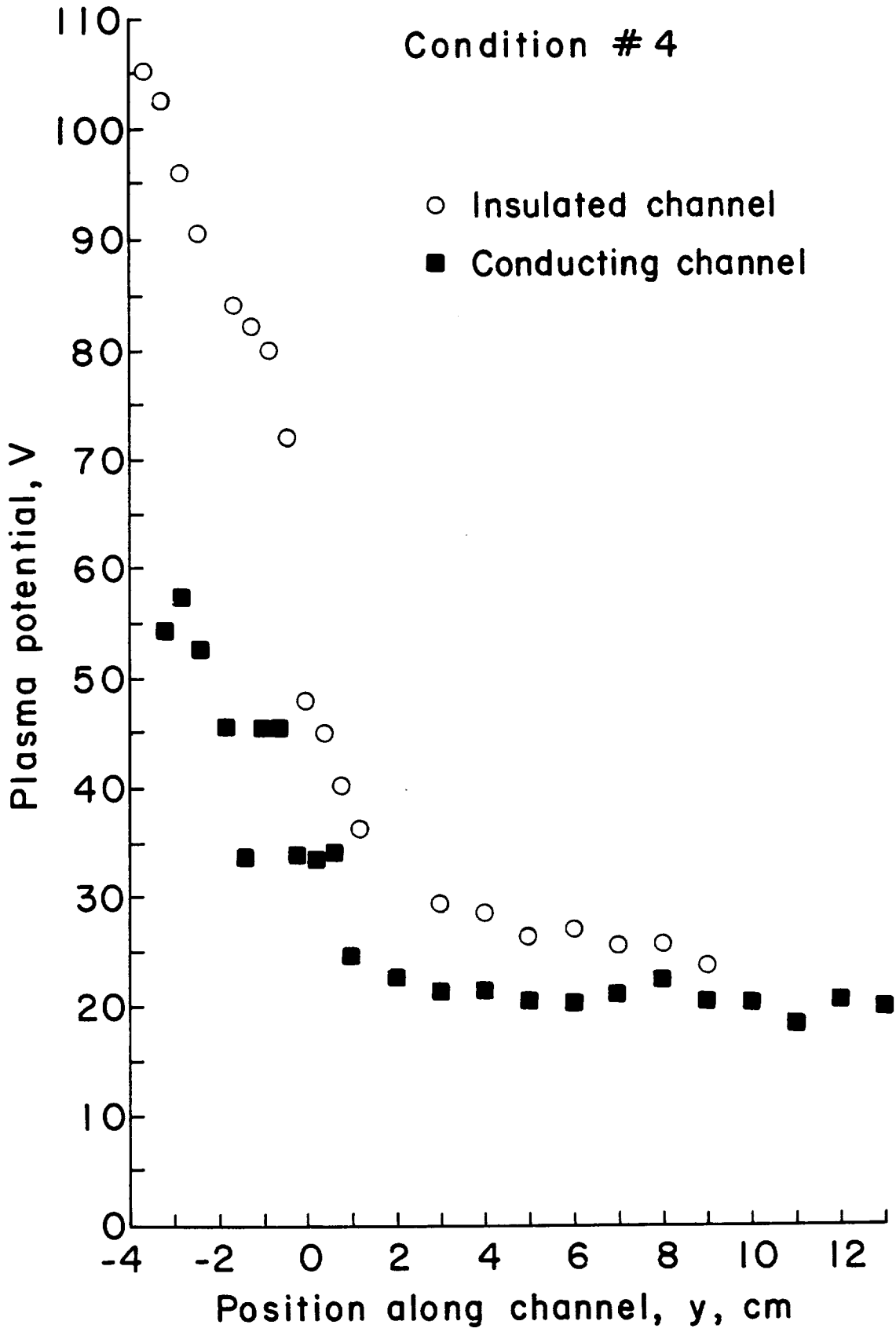

Fig. 16. Plasma potential as a function of position along the channel for condition 4 for insulated and conducting channels.

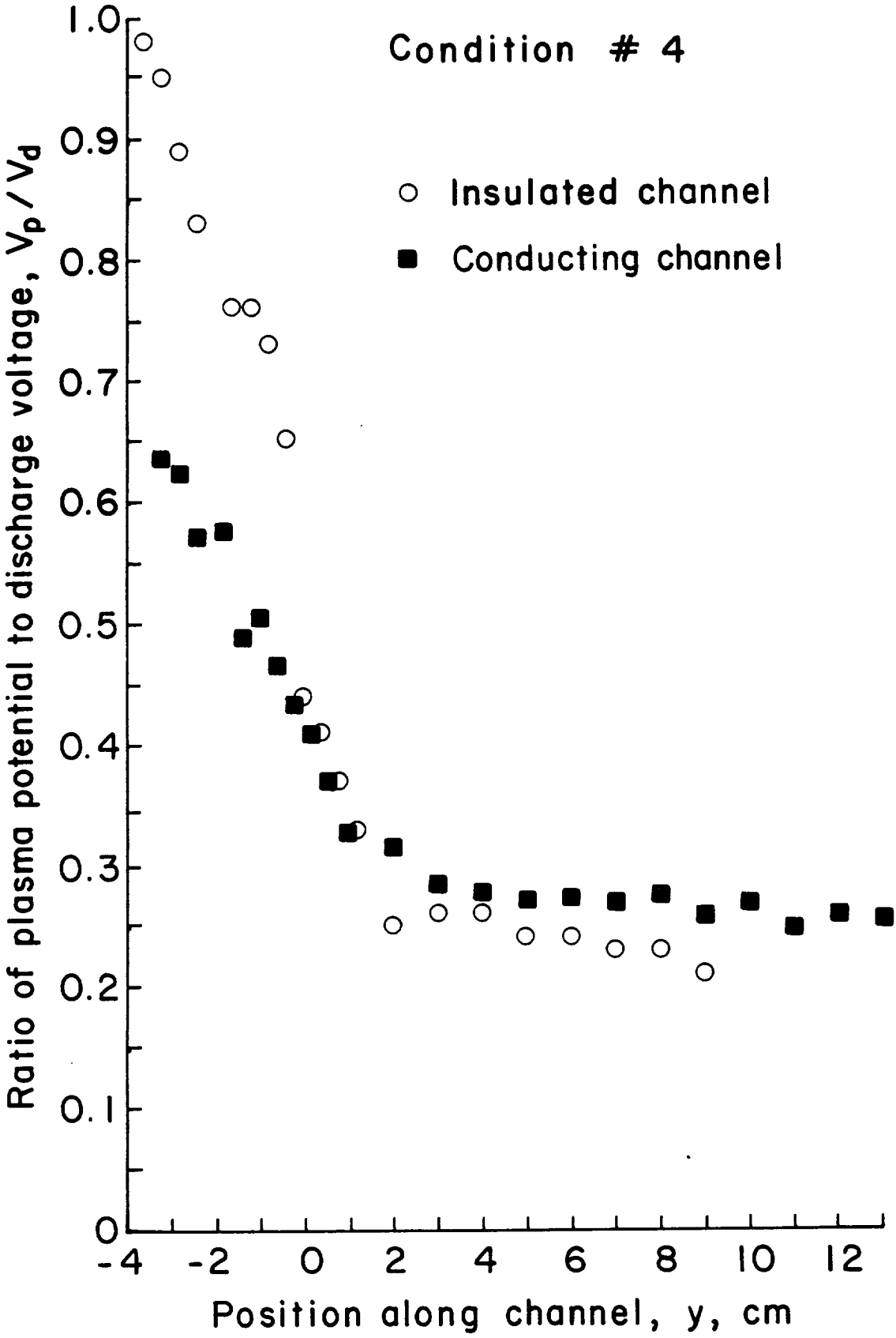

Fig. 17. Ratio of plasma potential to discharge voltage as a function of position along the channel for condition 4.

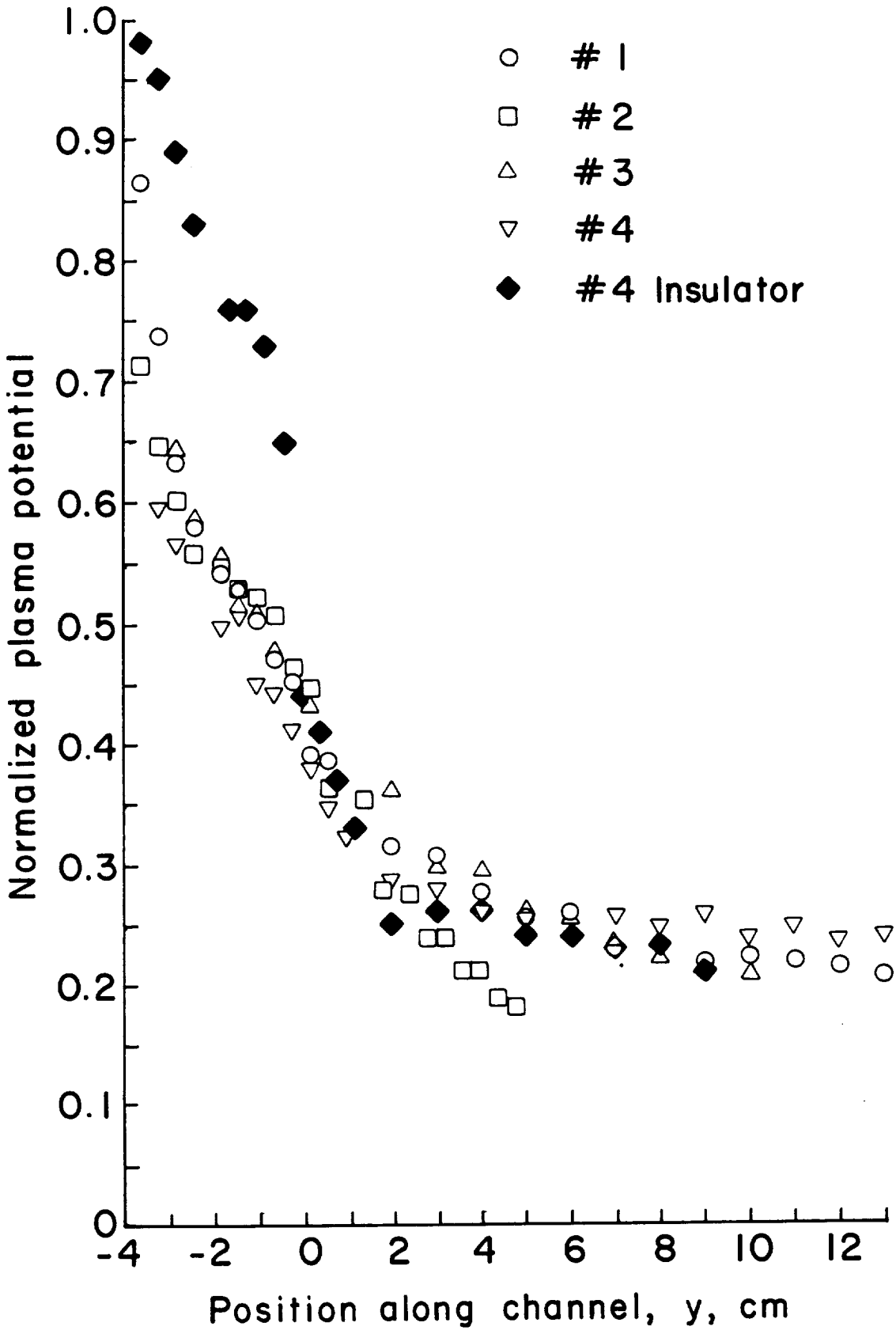

Fig. 18. Normalized plasma potential as a function of channel position.

determined by the operating conditions of the thruster. The four test conditions with the grounded channel required different normalization factors based on the different discharge power levels and magnetic field profiles. The second and more important point is that the profile of the plasma potential is a function of channel geometry only. The plasma potential profile for the four grounded channel tests converged after normalization, whereas the insulated channel profile has a significantly higher slope after normalization.

Beam Analysis

An analysis of the beam characteristics was conducted for the four selected operating conditions with grounded channel walls, as well as for conditions 3 and 4 with insulated channel walls. Integrated beam current and beam energy distribution data for these conditions is presented in Table 7. The grounded channel data exhibits a uniform behavior in all parameters for increasing power levels. The insulated channel data for test conditions 3 and 4 indicate a significant improvement in thruster efficiency was achieved by installing the pyrex liners. The enhanced electron temperature gradient and near discontinuous jump in potential at the acceleration channel permitted more

Table 7. Beam Current and Beam Energy Data for Grounded and Insulated Channel Tests

Condition No.	Integrated Beam Current, mA	E_{mean}, eV	σ, eV	E_{mean}/σ	E_{mean}/V_{dis}
1-grounded channel	1109	54.5	17	3.21	0.59
2-grounded channel	1090	52.5	10.5	5.00	0.68
3-grounded channel	400	40.0	10	4.00	0.60
3-insulated channel	510	54.0	12.5	4.32	0.69
4-grounded channel	515	44.5	16	2.78	0.55
4-insulated channel	699	64.5	17.5	3.69	0.56

effective use of the energy of the backstreaming electrons to generate ions. An increase in beam current of 28-36 percent and average beam energy of 35-45 percent was achieved with the insulated channel configuration for test conditions 3 and 4. Figure 19 presents the beam energy analysis for condition 4 for the grounded and insulated channel walls.

Thruster Characteristics

Closed-drift thrusters are inherently high discharge-power-operation devices. Current densities on the order of A/cm^2 are required to obtain useful propellant efficiencies. This investigation was focused on understanding the ion generation and acceleration processes of the device so that future modifications to the design may be made to improve the overall efficiency. Power supply limitations did not permit operation in a regime which could have established significantly higher thruster efficiencies by improving the propellant and power efficiencies. However, tests conducted with xenon have demonstrated propellant efficiencies in excess of 64 percent. The tendencies of increasing beam current and beam energy with discharge power, along with design modifications that improve energy utilization of backstreaming electrons, suggests that operation in the 1400-1800 s specific impulse range with thruster efficiencies above 40 percent is attainable.

V. SUMMARY OF RESULTS

A review of the orbit-raising capabilities of a 1000-2000 s specific impulse range device operating at modest efficiencies indicated that closed-drift thruster technology may provide significant performance advantages over other forms of electric propulsion. This

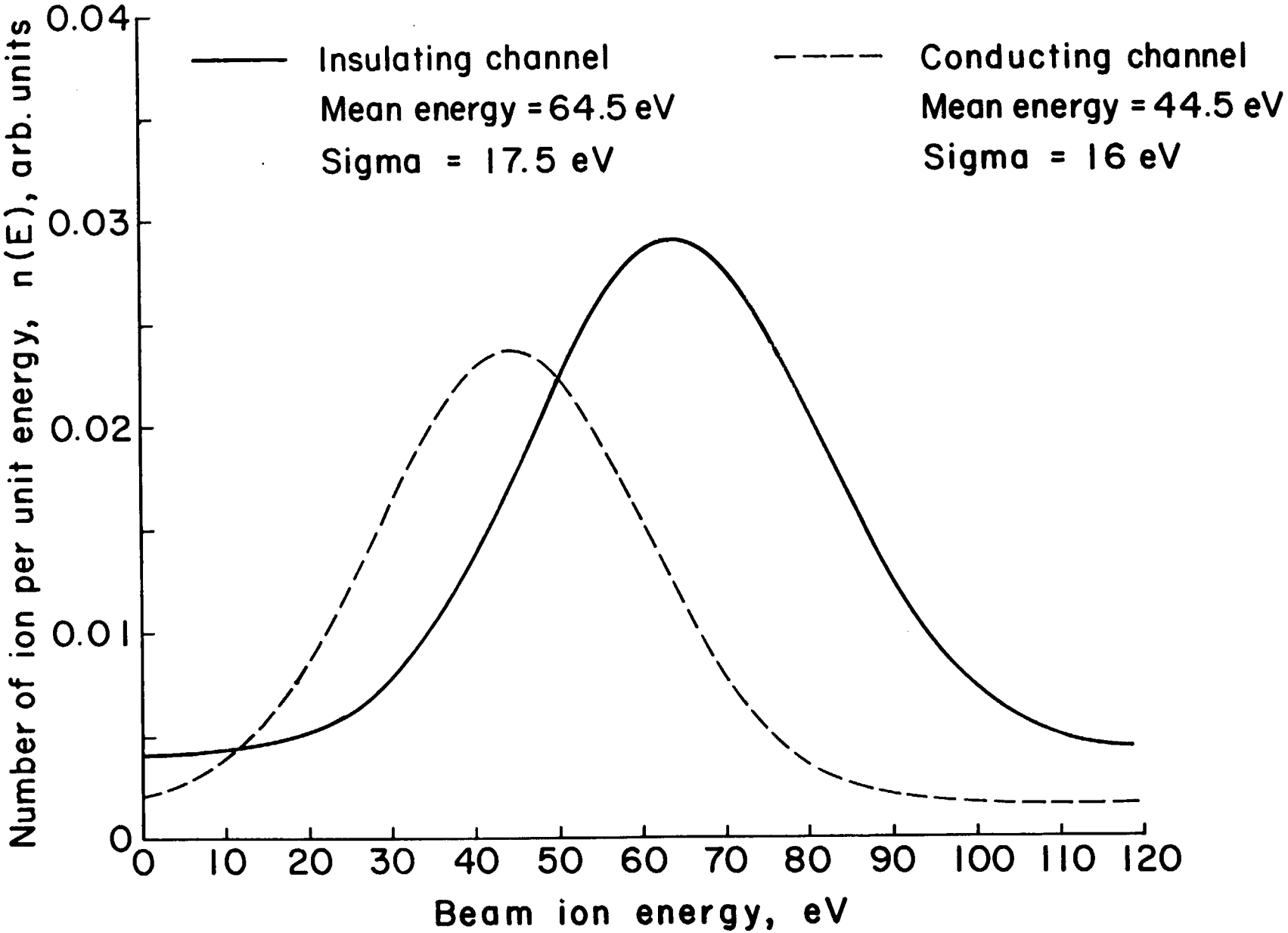

Fig. 19. Beam energy analysis for condition 4 for conducting and insulating channels.

is, in part, a consequence of the potentially higher thrust density and low specific mass associated with closed-drift thrusters.

A second-generation closed-drift thruster was designed and tested to enhance understanding of the ion generation and acceleration processes involved. The thruster employed an electromagnet to vary the magnetic field profile so that the propellant efficiency could be optimized at a desired operating point by more efficient use of the electron energy to produce ions. The radial magnetic field component variation with axial position along the channel was designed so as to accommodate the conflicting requirements of ion production and acceleration.

Faraday and Langmuir probe systems were built to provide information about the beam and discharge plasmas. Preliminary discharge characterization indicated a normal increase in channel conductivity with increasing propellant flow. The discharge operating regime was limited in one way by the maximum voltage of the discharge power supply. Another limitation was the minimum flow required to sustain a discharge, which was about 23-24 sccm for all operating conditions. The data also indicated an increase in channel conductivity going from the short channel to the long channel configuration. This increased channel conductivity was interpreted as an increase in ionization efficiency associated with a larger ion production volume for the long channel configuration. Preliminary analysis of beam characteristics for a range of discharge and magnet currents indicated that the ion generation process in the channel was becoming more effective at higher power levels relative to generation further downstream. An analysis of the ion beam energy distribution indicated a Gaussian

profile whose mean energy represented an increasing fraction of the discharge voltage for higher discharge voltages.

Based on the initial analysis of the discharge and beam characteristics, four operating conditions of the long channel thruster were selected for Langmuir probe diagnostics of the acceleration channel, and further beam energy analysis. Detailed Langmuir probing of the thruster channel indicated that the Maxwellian electron density exhibited a peaked profile in the high magnetic field acceleration region which dropped off rapidly beyond the field region. Primary electron densities also exhibited a peaked profile in the same region. This indicated that the maximum ionization was taking place just inside the magnetic field with the bulk of ion production occurring downstream of the grounded channel. Electron temperature profiles indicated a higher temperature electron population in the acceleration channel and ion production region than that measured in the downstream beam region. This thruster was thus operating at a condition between the two theoretical extremes of constant electron temperature and strict energy conservation delivering all directed electron energy as thermal energy upstream. The plasma potential profile rose sharply in the strongest magnetic field region where greatest resistance to electron conduction was encountered and generally rose as the anode was approached.

Further inspection of electron temperature profiles indicated that the grounded channel walls were acting as a virtual anode, thus creating a loss mechanism for the plasma. Because of this, dielectric cylinders of pyrex were placed in the thruster to line the inner and outer metal channel walls. This resulted in a steep electron temperature gradient along the channel and a near discontinuous plasma

potential jump at the positive end of the acceleration channel. This operation corresponded to a closed-drift anode-layer accelerator. An increase in beam current of 28-36 percent and average beam energy of 35-45 percent was achieved with the insulated channel configuration. Normalized plasma potential as a function of channel position indicated that the magnitude of the plasma potential is a function of the operating conditions of the thruster, but the profile is a function of channel geometry only.

Power-supply limitation did not permit operation in a regime which could have established significantly higher thruster efficiencies by improving power and propellant efficiencies. However, the tendencies of increasing beam current and beam energy with discharge power, along with design modifications that improve energy utilization of back-streaming electrons, suggests that operation in the 1400-1800 s specific impulse range with modest efficiencies is attainable.

REFERENCES

1. A. I. Morozov, Yu. V. Esipchuk, G. N. Ticinin, A. V. Trofinov, Yu. A. Sharov, and G. Ya. Shahepkin, "Plasma Acceleration with Closed Electron Drift and Extended Acceleration Zone," Sov. Phys.-Tech. Phys., Vol. 17, pp. 38-45, July 1972.

2. V. I. Garkusha, V. S. Yerofeyev, Ye. A. Lyapin, and S. P. Chugina, "Characteristics of a Single-Stage Cesium Anode-Layer Accelerator," (in Russian), Abstract for IV All-Union Conference on Plasma Accelerators and Ion Injectors, pp. 25-26, Moscow, 1978.

3. G. M. Plank, "Experimental Investigation of a Hall-Current Accelerator," NASA Contr. Report CR-168133, Jan. 1983.

4. Kaufman, H. R. and Robinson, R. S., "Low Specific Impulse Electric Thrusters," NASA Contr. Report CR-174678, July 1984.

5. Kaufman, H. R. and R. S. Robinson, "Electric Thruster Performance for Orbit-Raising and Maneuvering," in Orbit Raising and Maneuvering Propulsion: Research Status and Needs, edited by L. H. Caveny, Vol.89 of Progress in Astronautics and Aeronautics, 303-326, 1984.

6. V. K. Rawlin and M. J. Patterson, "Performance of 30 cm Xenon Ion Thrusters," AIAA-85-2009, Sept. 1985.

7. Kaufman, H. R. and Robinson, R. S., "Electric Propulsion for Upper Stage/Transfer Vehicle," NASA CR-168022, Sept. 1982.

8. Kaufman, H. R., "Technology of Closed-Drift Thrusters," AIAA-83-1398, June 1983.

9. Brophy, J. R., and P. J. Wilbur," Application of an Ion Thruster Performance Model to Orbit Transfer Mission Analysis, AIAA-85-1150.

10. Kaufman, H. R., "Theory of Ion Acceleration with Closed Electron Drift," J. Spacecr. Roc., Vol. 21, No. 6, 558-562, 1984.